Chaos and Order in Event-Triggered Control

Gleizer, Gabriel de Albuquerque; Mazo, Manuel

DOI
10.1109/TAC.2023.3242334

Publication date
2023

Document Version
Final published version

Published in
IEEE Transactions on Automatic Control

Chaos and Order in Event-Triggered Control

Gabriel de Albuquerque Gleizer, *Member, IEEE*, and Manuel Mazo Jr., *Senior Member, IEEE*

***Abstract*—Event-triggered control (ETC) is claimed to provide significant reductions in sampling frequency when compared to periodic sampling, but little is formally known about its generated traffic. This work shows that ETC can exhibit very complex, even chaotic traffic, especially when the triggering condition is aggressive in reducing communications. First, by looking at the map dictating the evolution of states sampled, we characterize limit traffic patterns by observing invariant lines and planes through the origin, as well as their attractivity. Then, we present abstraction-based methods to compute limit metrics, such as limit average and limit inferior intersample time of periodic ETC (PETC), with considerations to the robustness of such metrics, as well as measuring the emergence of chaos. The methodology and tools allow us to find ETC examples that provably outperform periodic sampling in terms of average IST. In particular for PETC, we prove that this requires aperiodic or chaotic traffic.**

***Index Terms*—Chaotic systems, computational methods, event-triggered control (ETC), hybrid systems, sampled-data control.**

I. Introduction

SINCE the seminal paper from [1], event-triggered control (ETC) has been considered a disruptive method for sampled-data control implementations over digital media. The astonishingly simple design and stability analysis methods proposed by Tabuada cast new light on the idea of aperiodic sampling, which had been studied since the 1950s [2] and gained renewed interest in the early 2000s [3]. The idea behind ETC is natural: instead of sampling periodically, sample only when "needed" based on some significant event; therefore, massive reductions in communications, as well as in energy of battery-powered motes, can be achieved, enabling new control applications with cheap hardware, or larger networks of control systems. Unsurprisingly, immense interest followed, and a lot of effort was dedicated in the following years to design better event-triggering mechanisms [4], [5], e.g., perturbed systems, extend applications to output-feedback control [6], or make implementations more practical, as the periodic ETC (PETC) from [7], where events are checked periodically.

Manuscript received 9 February 2022; revised 12 February 2022 and 10 November 2022; accepted 26 January 2023. Date of publication 6 February 2023; date of current version 26 October 2023. This work was supported by the European Research Council through the SENTIENT under project ERC-2017-STG #755953. Recommended by Associate Editor D. Antunes. *(Corresponding author: Gabriel de Albuquerque Gleizer.)*

The authors are with the Delft Center for Systems and Control, Delft Technical University, 2628 CD Delft, The Netherlands (e-mail: g.gleizer@tudelft.nl; m.mazo@tudelft.nl).

Color versions of one or more figures in this article are available at https://doi.org/10.1109/TAC.2023.3242334.

Digital Object Identifier 10.1109/TAC.2023.3242334

While understanding of the ETC's control performance and stability has reached a high level of maturity, thanks also to the hybrid-systems formalism of [8], the comprehension of ETC's sampling patterns and performance is severely lacking. Critically, how much bandwidth can ETC save compared to, e.g., periodic sampling? What is an ETC's average *intersample time* (IST)? Most ETC papers focus only on estimating a lower bound for the *minimum intersample time* (MIST), to prove the absence of Zeno behavior. Unfortunately, the MIST is often conservative and does not prove that the ETC's performance is better than a well-designed periodic sampling time. Unsurprisingly, nearly all ETC papers contain numerical simulations showing IST trajectories and their average statistics, to give evidence of ETC's practical relevance.

Comparatively, much less effort has been put to model ETC's generated traffic. We split the existing literature into two categories.[1] The first category aims at understanding asymptotic properties of ETC's ISTs qualitatively [10], [11], [12], [13], which are mostly dedicated to two-dimensional linear time-invariant (LTI) systems. The earliest work in this category is [10], which analyses equilibrium ISTs, and is the first (possibly only) to notice the emergence of chaotic behavior when using the triggering condition of [1]. The other works are much more recent, and provide conditions to show when traffic converges to periodic sampling or oscillatory patterns. In particular, Postoyan et al. [13] allows us to approximately compute average intersample for such planar systems when the triggering parameters are sufficiently small. The second category aims at taming the highly variable ISTs of ETC for scheduling purposes, relying on finite-state models (abstractions) under the framework of [14]. Such models have been developed for continuous ETC (CETC) for LTI systems in [15], [16], PETC [17], [18], and nonlinear systems [19], [20], while only [21], [22], [23] address longer-term traffic predictions. In particular, the authors in [22] and [23] developed tools to compute the smallest (across initial states) average intersample time (SAIST) of an LTI PETC system, by using weighted automata [24] as abstractions.

There are issues involved in both the qualitative and quantitative analyzes in the present literature. On the quantitative side, the obtained metrics lack a sense of robustness: that is, a given PETC system may have a SAIST of, e.g., 1 time unit, which may be only attained from a negligible, 0-measure subset of initial conditions. If all other initial states lead to some other traffic pattern with higher SAIST, e.g., 3, this much higher value is clearly a more representative performance metric. In addition, as noted in [10] and investigated here, ETC systems can exhibit

[1]It is also worth mentioning the approach of [9], which proposed an event-triggering mechanism that ensures given traffic criteria in terms of a token bucket model. Although very interesting, we veer away from this approach because it is unclear whether adding conditions to enforce traffic patterns could actually degrade the sampling performance of the original mechanism.

chaotic traffic, and as such a stable representative traffic pattern may not be found. This hints on a problem of the qualitative side of the literature, which more recently has ignored the emergence of chaotic traffic. This also forces us to carefully define robust metrics for ETC before attempting to compute them.

This work expands the qualitative understanding of ETC's asymptotic traffic patterns and bridge it to the quantitative approach of [22], [23], focusing on LTI systems with zero-order-hold state feedback and a common class of quadratic triggering conditions [7]. For that, we first characterize limit metrics of interest, such as limit inferior and limit average, and observe that they are related to the asymptotic properties of the traffic. This is the starting point for our main contributions:

1) presenting limit behaviors of LTI ETC systems and methods to compute them, not limited to $\mathbb{R}^2$;
2) classifying limit behaviors in terms of stable versus unstable, periodic versus aperiodic, orderly versus chaotic;
3) based on this, expanding the results from [22], [23] for PETC to compute robust metrics.

We propose auxiliary concepts and obtain results that may be useful on their own right:

1) we show that if a PETC that renders the origin globally asymptotically stable (GES) converges to a periodic traffic pattern, then this traffic pattern can be used as a (multirate) periodic sampling schedule (Proposition 9)—this does not necessarily happen to CETC;
2) we provide a stability characterization for outputs of a system, when these outputs come from a finite set;
3) we present the notion of behavioral entropy (Def. 17) as a measure of chaos of a system's output trajectories, how to compute this quantity in an abstraction (Theorem 8), and show that this quantity is an upper bound of the concrete system's (Proposition 12).

The rest of this article is organized as follows. Section III presents the basic ETC formulation, how ISTs can be computed, and the main problem statement. The qualitative side of the work, presenting limiting behaviors and their general properties is given in Section IV, where we are able to establish conditions for which periodic patterns occur and the associated states that generate them. In doing that, we explore their local attractivity and the emergence of chaotic invariant sets. This paves the way for the quantitative side of this work in Section V using symbolic abstractions, where we properly define robust limit metrics for PETC taking chaos into consideration, provide methods to estimate PETC's behavioral entropy using the abstraction, establish when traffic patterns are not involved in chaos, and describe how to estimate the desired robust limit metrics. Numerical examples are given in Section VI. Finally, Section VII concludes this article with discussions about the presented results.

II. Mathematical Preliminaries

We denote by $\mathbb{N}_0$ the set of natural numbers including zero, $\mathbb{N} := \mathbb{N}_0 \setminus \{0\}$, $\mathbb{N}_{\leq n} := \{1, 2, \ldots, n\}$, and $\mathbb{R}_+$ the set of nonnegative reals. We denote by $|\boldsymbol{x}|$ the norm of a vector $\boldsymbol{x} \in \mathbb{R}^n$, but if s is a sequence or set, $|s|$ denotes its length or cardinality, respectively. For a square matrix $\boldsymbol{A} \in \mathbb{R}^{n\times n}$, $\lambda(\boldsymbol{A}) \subset \mathbb{C}^n$ is the set of its eigenvalues, and $\lambda_i(\boldsymbol{A})$ is the ith largest-in-magnitude. The complex conjugate of $z \in \mathbb{C}^n$ is denoted by z^*. The set $\mathbb{S}^n$ denotes the set of symmetric matrices in $\mathbb{R}^n$. For $\boldsymbol{P} \in \mathbb{S}^n$, we write $\boldsymbol{P} \succ \boldsymbol{0}$ ($\boldsymbol{P} \succeq \boldsymbol{0}$) if $\boldsymbol{P}$ is positive definite (semidefinite); $\lambda_{\max}(\boldsymbol{P})$ ($\lambda_{\min}(\boldsymbol{P})$) denotes its maximum (minimum) eigenvalue. For a set $\mathcal{X} \subseteq \Omega$, we denote by $\mathrm{cl}(\mathcal{X})$ its closure, $\partial\mathcal{X}$ its boundary, and $\bar{\mathcal{X}}$ its complement: $\Omega \setminus \mathcal{X}$. We often use a string notation for sequences, e.g., $\sigma = abc$ reads $\sigma(1) = a, \sigma(2) = b, \sigma(3) = c$. Powers and concatenations work as expected, e.g., $\sigma^2 = \sigma\sigma = abcabc$. In particular, σ^ω denotes the infinite repetition of σ. An infinite sequence of numbers is denoted by $\{a_i\} := a_0, a_1, a_2, \ldots$. We apply a function $f : \mathcal{X} \to \mathcal{Y}$ to a set $\mathcal{A} \subseteq \mathcal{X}$ the usual way, $f(\mathcal{A}) := \{f(\boldsymbol{x}) \mid \boldsymbol{x} \in \mathcal{A}\}$. For a relation $\mathcal{R} \subseteq \mathcal{X}_a \times \mathcal{X}_b$, its inverse is denoted as $\mathcal{R}^{-1} = \{(x_b, x_a) \in \mathcal{X}_b \times \mathcal{X}_a \mid (x_a, x_b) \in \mathcal{R}\}$.

An autonomous system $\dot{\boldsymbol{\xi}}(t) = f(\boldsymbol{\xi}(t))$ is said to be GES if there exist $M \in [1, \infty)$ and $b > 0$ such that all of its solutions satisfy $|\boldsymbol{\xi}(t)| \leq M\mathrm{e}^{-bt}|\boldsymbol{\xi}(0)|$ for every initial state $\boldsymbol{\xi}(0)$. When needed to avoid ambiguity, we use $\boldsymbol{\xi}_{\boldsymbol{x}}(t)$ to denote a trajectory from initial state $\boldsymbol{\xi}(0) = \boldsymbol{x}$.

A. Chaos

Consider the map $f : \mathcal{X} \to \mathcal{X}$, where $\mathcal{X}$ is a metric space, and the discrete-time system (or recursion) $\boldsymbol{x}(k+1) = f(\boldsymbol{x}(k))$. A set $\mathcal{Y} \subset \mathcal{X}$ is said to *fixed* or *invariant* if $f(\mathcal{Y}) = \mathcal{Y}$, *forward invariant* if $f(\mathcal{Y}) \subseteq \mathcal{Y}$, and *periodic* if there is some $m \in \mathbb{N}$ such that $f^m(\mathcal{Y}) = \mathcal{Y}$. The *forward orbit* of a point $\boldsymbol{x}$ is $\mathcal{O}(\boldsymbol{x}) := \{f^k(\boldsymbol{x}) \mid k \in \mathbb{N}_0\}$. Obviously, every forward orbit is forward invariant. Whilst there are multiple slightly different definitions of chaos, we use the concept of [25], which relies on the notions of *transitivity* and *sensitivity to initial conditions.*

Definition 1 (Transitivity [25, Sec. 2.5]): A map $f : \mathcal{X} \to \mathcal{X}$ is said to be *(topologically) transitive* on an invariant set $\mathcal{Y}$ if the forward orbit of some point $p \in \mathcal{X}$ is dense in $\mathcal{Y}$. From the Birkhoff Transitivity Theorem, this is equivalent to the following property: for every two open subsets $\mathcal{U}$ and $\mathcal{V}$ of $\mathcal{Y}$, there is a positive integer n such that $f^n(\mathcal{U}) \cap \mathcal{V} \neq \emptyset$.

If f is transitive, points starting arbitrarily close to each other can drift away but will come arbitrarily close back to each other after enough iterations.

Definition 2 (Sensitivity to initial conditions [25, Sec. 3.5]): A map $f : \mathcal{X} \to \mathcal{X}$, $\mathcal{X}$ being a metric space, is said to be *sensitive to initial conditions* on an invariant set $\mathcal{Y} \subseteq \mathcal{X}$ if there is an $r > 0$ such that, for each point $\boldsymbol{x} \in \mathcal{Y}$ and for each $\epsilon > 0$, there exists a point $\boldsymbol{y} \in \mathcal{Y}$ satisfying $d(\boldsymbol{x}, \boldsymbol{y}) < \epsilon$ and a $k \in \mathbb{N}$ with $d(f^k(\boldsymbol{x}), f^k(\boldsymbol{y})) \geq r$.

Definition 3 (Chaos [25, Sec. 3.5]): A map $f : \mathcal{X} \to \mathcal{X}$, $\mathcal{X}$ being a metric space, is said to be *chaotic on an invariant set* $\mathcal{Y}$ provided (i) f is transitive on $\mathcal{Y}$, and (ii) f is sensitive to initial conditions on $\mathcal{Y}$.

In case a chaotic system is additionally *ergodic*,[2] the celebrated Birkhoff Ergodic Theorem is particularly useful when one is interested in limit average metrics.

Theorem 1 (Birkhoff Ergodic Theorem [25]): Assume $f : \mathcal{X} \to \mathcal{X}$ is an ergodic function with ergodic measure μ, and let $g : \mathcal{X} \to \mathbb{R}$ be a μ-integrable function. Then,

$$\lim_{n\to\infty} \frac{1}{n+1} \sum_{i=1}^{n} g \circ f^i(x) = \int_{\mathcal{X}} g(x)\mathrm{d}\mu(x)$$

for μ-almost every x.

[2]See [25] for a rigorous definition of ergodicity. We skip the definition and present a simplified version of the Birkhoff Ergodic Theorem due to readability and space considerations.

As a consequence, if f is ergodic and μ is well-behaved,[3] the iteration-average (left-hand side of the expression above) converges to the same value from almost every initial condition.

B. Invariants of Linear Systems

Most of the analysis of limit behaviors of (P)ETC on linear systems involve studying invariants of linear systems, their stability and relationship with quadratic cones. Here, we provide some definitions and results on this topic.

Definition 4 (Homogeneous set): A set $\mathcal{Q} \subseteq \mathbb{R}^n$ is called *homogeneous* if $\boldsymbol{x} \in \mathcal{Q} \Rightarrow \lambda \boldsymbol{x} \in \mathcal{Q}, \forall \lambda \in \mathbb{R} \setminus \{0\}$.

For the next results, we borrow a few definitions from previous work [23] concerning square matrices.

Definition 5 (Mixed matrix [23]): Consider a matrix $\boldsymbol{M} \in \mathbb{R}^{n\times n}$ and let $\lambda_i, i \in \mathbb{N}_{\leq n}$ be its eigenvalues sorted such that $|\lambda_i| \geq |\lambda_{i+1}|$ for all i. We say that $\boldsymbol{M}$ is *mixed* if, for all $i < n$, $|\lambda_i| = |\lambda_{i+1}|$ implies that $\Im(\lambda_i) \neq 0$ and $\lambda_i = \lambda_{i+1}^*$.

Mixed matrices are diagonalizable and do not have distinct eigenvalues of the same magnitude, with the exception of pairs of complex conjugate eigenvalues.

Definition 6 (Matrix of irrational rotations [23]): A matrix $\boldsymbol{M} \in \mathbb{R}^{n\times n}$ is said to be of *irrational rotations* if the arguments of all of its complex eigenvalues are irrational multiples of π.

The set of mixed matrices of irrational rotations is of full Lebesgue measure in the set of square matrices [23], and as such these matrices can be considered generic.

Proposition 1 presents a simple way to verify whether a linear subspace is a subset of a quadratic cone.

Proposition 1 (see [22]): Let $\mathcal{A}$ be a linear subspace with basis $\boldsymbol{v}_1, \boldsymbol{v}_2, \ldots, \boldsymbol{v}_m$, and let $\boldsymbol{V}$ be the matrix composed of the vectors $\boldsymbol{v}_i$ as columns. Let $\boldsymbol{Q} \in \mathbb{S}^n$ be a symmetric matrix and define $\mathcal{Q}_{\geq} := \{\boldsymbol{x} \in \mathbb{R}^n \mid \boldsymbol{x}^\mathsf{T}\boldsymbol{Q}\boldsymbol{x} \geq 0\}$, $\mathcal{Q}_{>} := \{\boldsymbol{x} \in \mathbb{R}^n \mid \boldsymbol{x}^\mathsf{T}\boldsymbol{Q}\boldsymbol{x} > 0\}$ and $\mathcal{Q}_{=} := \{\boldsymbol{x} \in \mathbb{R}^n \mid \boldsymbol{x}^\mathsf{T}\boldsymbol{Q}\boldsymbol{x} = 0\}$. Then, $\mathcal{A} \setminus \{\boldsymbol{0}\} \subseteq \mathcal{Q}_{\geq}$ (resp. $\mathcal{Q}_{>}$ and $\mathcal{Q}_{=}$) if and only if $\boldsymbol{V}^\mathsf{T}\boldsymbol{Q}\boldsymbol{V} \succeq \boldsymbol{0}$ (resp. $\boldsymbol{V}^\mathsf{T}\boldsymbol{Q}\boldsymbol{V} \succ \boldsymbol{0}$ and $\boldsymbol{V}^\mathsf{T}\boldsymbol{Q}\boldsymbol{V} = \boldsymbol{0}$).

III. ETC and its Traffic

A. Traffic Models of ETC Systems

Consider a closed-loop linear system

$$\begin{aligned} \dot{\boldsymbol{\xi}}(t) &= \boldsymbol{A}\boldsymbol{\xi}(t) + \boldsymbol{B}\boldsymbol{K}\hat{\boldsymbol{\xi}}(t), \\ \boldsymbol{\xi}(0) &= \hat{\boldsymbol{\xi}}(0) = \boldsymbol{x}_0, \end{aligned} \tag{1}$$

which is a sampled-data state feedback with zero-order hold: the state $\boldsymbol{\xi}(t) \in \mathbb{R}^{n_\mathsf{x}}$ is sampled at instants $t_i, \forall i \in \mathbb{N}$, and held constant for feedback, which makes the state signal used for control $\hat{\boldsymbol{\xi}}$ satisfy $\hat{\boldsymbol{\xi}}(t) = \boldsymbol{\xi}(t_i), \forall t \in [t_i, t_{i+1})$. Matrices $\boldsymbol{A}, \boldsymbol{B}, \boldsymbol{K}$ have appropriate dimensions.

In ETC, a *triggering condition* determines the sequence of times t_i. In PETC, this condition is checked only periodically, with a fundamental checking period h. The sampling time t_{i+1}, hence, assumes the following form:

$$t_{i+1} = \inf\{t \in \mathcal{T} \mid t > t_i \text{ and } c(t - t_i, \boldsymbol{\xi}(t), \hat{\boldsymbol{\xi}}(t))\}, \tag{2}$$

where $c : \mathcal{T} \times \mathbb{R}^{n_\mathsf{x}} \times \mathbb{R}^{n_\mathsf{x}} \to \{\text{true}, \text{false}\}$ is the *triggering condition*, and $\mathcal{T}$, the set of checking times, is $\mathbb{R}_+$ for CETC and $h\mathbb{N}$ for PETC. We consider the family of *quadratic triggering conditions* from [7] with an additional maximum interevent time condition as follows:

$$c(s, \boldsymbol{x}, \hat{\boldsymbol{x}}) := \begin{bmatrix} \boldsymbol{x} \\ \hat{\boldsymbol{x}} \end{bmatrix}^\mathsf{T} \boldsymbol{Q}(s) \begin{bmatrix} \boldsymbol{x} \\ \hat{\boldsymbol{x}} \end{bmatrix} > 0 \text{ or } s \leq \bar{\tau} \tag{3}$$

where $\boldsymbol{Q} : \mathcal{T} \to \mathbb{S}^{2n_\mathsf{x}}$ is the designed triggering matrix function (possibly constant), and $\bar{\tau}$ is the chosen maximum interevent time.[4] When $\mathcal{T} = \mathbb{R}_+$, we assume $\boldsymbol{Q}$ is differentiable. Many of the triggering conditions available in the literature can be written as in (3); the interested reader may refer to [7] for a comprehensive list of quadratic triggering and stability conditions.

We are interested in modeling the traffic generated by (P)ETC, i.e., understanding how the ISTs evolve from different initial conditions. As noted in [18], the interevent time $t_{i+1} - t_i$ is solely a function of the ith sample $\boldsymbol{\xi}(t_i)$. First, note that, $\boldsymbol{\xi}(t)$ is a function of $\hat{\boldsymbol{\xi}}(t) = \boldsymbol{\xi}(t_i)$ and the elapsed time $s := t - t_i$

$$\begin{aligned} \boldsymbol{\xi}(t_i + s) &= \boldsymbol{M}(s)\boldsymbol{\xi}(t_i), \\ \boldsymbol{M}(s) &:= \boldsymbol{A}_\mathrm{d}(s) + \boldsymbol{B}_\mathrm{d}(s)\boldsymbol{K} := \mathrm{e}^{\boldsymbol{A}s} + \textstyle\int_0^s \mathrm{e}^{\boldsymbol{A}t}\mathrm{d}t\boldsymbol{B}\boldsymbol{K}. \end{aligned} \tag{4}$$

Now let $\tau : \mathbb{R}^{n_\mathsf{x}} \to (0, \bar{\tau}] \cap \mathcal{T}$ be the interevent time function, i.e., for every state $\boldsymbol{x} \in \mathbb{R}^{n_\mathsf{x}}$, τ must return the value of $t_{i+1} - t_i$. It follows from (2) to (4) that

$$\begin{aligned} \tau(\boldsymbol{x}) &= \inf\left\{s \in \mathcal{T} \mid \boldsymbol{x}^\mathsf{T}\boldsymbol{N}(s)\boldsymbol{x} > 0 \text{ or } s = \bar{\tau}\right\}, \\ \boldsymbol{N}(s) &:= \begin{bmatrix} \boldsymbol{M}(s) \\ \mathbf{I} \end{bmatrix}^\mathsf{T} \boldsymbol{Q}(s) \begin{bmatrix} \boldsymbol{M}(s) \\ \mathbf{I} \end{bmatrix}, \end{aligned} \tag{5}$$

where $\mathbf{I}$ denotes the identity matrix. Thus, the event-driven evolution of sampled states can be compactly described by the recurrence

$$\boldsymbol{\xi}(t_{i+1}) = \boldsymbol{M}(\tau(\boldsymbol{\xi}(t_i)))\boldsymbol{\xi}(t_i). \tag{6}$$

Throughout this article, we refer to the function above as the *sample system*, using the shortened version

$$\begin{aligned} \boldsymbol{x}_{i+1} &= f(\boldsymbol{x}_i), \\ y_i &= \tau(\boldsymbol{x}_i), \end{aligned} \tag{7}$$

where $\boldsymbol{x}_i := \boldsymbol{\xi}(t_i)$ and $f(\boldsymbol{x}) := \boldsymbol{M}(\tau(\boldsymbol{x}))\boldsymbol{x}$. The map is equipped with an output y which is the associated interevent time: for a traffic model, this is the output of interest. We shall denote the sequence of outputs from (7) for a given initial state $\boldsymbol{x}_0$ by $\{y_i(\boldsymbol{x}_0)\}$. We make the following assumption on the ETC system.

Standing Assumption: System (1)–(3) is non-Zeno, i.e., $\tau(\boldsymbol{x}) \geq \underline{\tau} > 0$ for all $\boldsymbol{x} \neq \boldsymbol{0}$. In addition, $f(\boldsymbol{x}) \neq \boldsymbol{0}$ for all $\boldsymbol{x} \neq \boldsymbol{0}$, i.e., the origin can only be reached (sample-wise) asymptotically.

Observe that it is standard in ETC design to prevent Zeno behavior. The value $\underline{\tau}$ is the system's MIST.

B. Isochronous Subsets in ETC

We start our analysis of sampling behaviors of ETC by studying the subsets of $\mathbb{R}^{n_\mathsf{x}}$ that generate the same IST. The first

[3] That is, $0 < \mu(x) < \infty$ for all x in the invariant set of interest; as a consequence μ-almost all are almost all.

[4] Often a maximum interevent time arises naturally from the closed-loop system itself (see [26]). Still, one may want to set a smaller maximum interevent time so as to establish a "heart beat" of the system.

characteristic to be highlighted is that ISTs are insensitive to magnitude.

Proposition 2 (Adapted from [27]): The sample system (7) is homogeneous; more specifically, for all $\lambda \in \mathbb{R} \setminus \{0\}, \tau(\lambda \boldsymbol{x}) = \tau(\boldsymbol{x})$ and $f(\lambda \boldsymbol{x}) = \lambda f(\boldsymbol{x})$.

Proof: Take any $\boldsymbol{x} \in \mathbb{R}^{n_x}$ and $\lambda \neq 0$; from (5), it holds that $\operatorname{sign}((\lambda \boldsymbol{x})^{\mathsf{T}} \boldsymbol{Q}(s)(\lambda \boldsymbol{x})) = \operatorname{sign}(\lambda^2 \boldsymbol{x}^{\mathsf{T}} \boldsymbol{Q}(s) \boldsymbol{x}) = \operatorname{sign}(\boldsymbol{x}^{\mathsf{T}} \boldsymbol{Q}(s) \boldsymbol{x})$, hence, $\tau(\lambda \boldsymbol{x}) = \tau(\boldsymbol{x})$. With this, $f(\lambda \boldsymbol{x}) = \boldsymbol{M}(\tau(\lambda \boldsymbol{x}))\lambda \boldsymbol{x} = \lambda \boldsymbol{M}(\tau(\boldsymbol{x}))\boldsymbol{x} = \lambda f(\boldsymbol{x})$. □

This fact implies that the sequence $\{y_i(\boldsymbol{x})\}$ is equal to $\{y_i(\lambda \boldsymbol{x})\}$, for any $\lambda \neq 0$. Hence, to determine whether ETC exhibits fixed (periodic) behavior, we need to verify which lines passing thorough the origin, or collections of lines, are invariant under f or under a finite iterate of f. Hereafter, we shall refer to lines that pass through the origin as *o-lines*.

Let us first look in detail what are the subsets of $\mathbb{R}^{n_x}$, which share the same (sequence of) interevent time(s).

Definition 7 (Isochronous and isosequential subsets): Consider system (7) and a sequence of ISTs $\sigma := s_1 s_2 \ldots s_m, s_i > 0$. We call the set of states $\boldsymbol{x} \in \mathbb{R}^n$ whose next m ISTs are $s_1, s_2, \ldots, s_m$ an *isosequential subset*, denoted by $\mathcal{Q}_\sigma$. When $m = 1$, we call it an *isochronous subset.*

By definition, when $\sigma = s$ is a singleton, $\mathcal{Q}_s = \{\boldsymbol{x} \in \mathbb{R}^{n_x} \mid \tau(\boldsymbol{x}) = s\}$; when $m > 1$, $\mathcal{Q}_\sigma$ can be obtained recursively as the set of states $\boldsymbol{x} \in \mathcal{Q}_{s_1}$ such that $\boldsymbol{M}(s_1)\boldsymbol{x} \in \mathcal{Q}_{s_2 \ldots s_m}$.

Proposition 3: Consider system (1)–(3) and a scalar $s > 0$. An isochronous subset $\mathcal{Q}_s$ can be characterized as

i) If $\mathcal{T} = \mathbb{R}_+$ (CETC) and $s < \bar{\tau}$, $\mathcal{Q}_s = \{\boldsymbol{x} \in \mathbb{R}^n \mid \boldsymbol{x}^{\mathsf{T}} \boldsymbol{N}(s) \boldsymbol{x} = 0$ and $\boldsymbol{x}^{\mathsf{T}} \boldsymbol{N}(s') \boldsymbol{x} \leq 0, \forall s' < s$ and $\boldsymbol{x}^{\mathsf{T}} \dot{\boldsymbol{N}}(s) \boldsymbol{x} > 0\}$.

ii) If $\mathcal{T} = h\mathbb{N}$ (PETC) and $s < \bar{\tau}$, $\mathcal{Q}_s = \{\boldsymbol{x} \in \mathbb{R}^n \mid \boldsymbol{x}^{\mathsf{T}} \boldsymbol{N}(s) \boldsymbol{x} > 0$ and $\boldsymbol{x}^{\mathsf{T}} \boldsymbol{N}(s') \boldsymbol{x} \leq 0, \forall s' < s, s' \in h\mathbb{N}\}$.

iii) $\mathcal{Q}_{\bar{\tau}} = \{\boldsymbol{x} \in \mathbb{R}^n \mid \boldsymbol{x}^{\mathsf{T}} \boldsymbol{N}(s') \boldsymbol{x} \leq 0, \forall s' < \bar{\tau}, s' \in \mathcal{T}\}$.

Proof: This is a trivial manipulation of (5), where in (i) we use the fact that $\boldsymbol{N}(s)$ is differentiable over $[0, \bar{\tau})$. □

Isosequential subsets are the intersection of an algebraic set with infinitely many semialgebraic sets for CETC; for PETC, it is the intersection of finitely many semialgebraic sets. We end this section with a result that simplifies the analysis for CETC under some special conditions.

Proposition 4: Consider system (7) and $\mathcal{T} = \mathbb{R}_+$ (CETC). If $\bar{\tau} = \inf\{s > 0 \mid \boldsymbol{N}(s) \succ \boldsymbol{0}\} < \infty$ and

$$\forall \boldsymbol{x} \in \mathbb{R}^{n_x} \setminus \{\boldsymbol{0}\}, s \in (0, \bar{\tau}], \boldsymbol{x}^{\mathsf{T}} \boldsymbol{N}(s) \boldsymbol{x} = 0 \Rightarrow \boldsymbol{x}^{\mathsf{T}} \dot{\boldsymbol{N}}(s) \boldsymbol{x} > 0$$

then

i) f and τ are differentiable;

ii) $\mathcal{Q}_s = \{\boldsymbol{x} \in \mathbb{R}^{n_x} \mid \boldsymbol{x}^{\mathsf{T}} \boldsymbol{N}(s) \boldsymbol{x} = 0\}, \forall s \in (0, \bar{\tau})$.

Proof: We first prove (ii), which is a lemma to (i).

ii) For any fixed $\boldsymbol{x} \neq \boldsymbol{0}$, consider the function $\phi_{\boldsymbol{x}}(s) = \boldsymbol{x}^{\mathsf{T}} \boldsymbol{N}(s) \boldsymbol{x}$, which is differentiable. If for some s, $\phi_{\boldsymbol{x}}(s) = 0$, we prove that all conditions from Proposition 3 (i) are satisfied; since $\dot{\phi}_{\boldsymbol{x}}(s) > 0$ by assumption, we need to prove that $\phi_{\boldsymbol{x}}(s') \leq 0, \forall s' < s$. Now, since $\phi_{\boldsymbol{x}}(s) = 0 \Rightarrow \dot{\phi}_{\boldsymbol{x}}(s) > 0$, from continuity, it holds that $\phi_{\boldsymbol{x}}(s^-) < 0$ for some $s^- < s$. For contradiction, assume $\phi_{\boldsymbol{x}}(s') > 0$ for some $s' < s^-$. Then, from Bolzano's theorem there is some point $s'' \in (s,' s^-)$ such that that $\phi_{\boldsymbol{x}}(s'') = 0$. One such s'' must have $\phi_{\boldsymbol{x}}(s'')$ cross zero from positive to negative, which implies $\dot{\phi}_{\boldsymbol{x}}(s'') \leq 0$, leading to a contradiction.

i) Now $\tau(\boldsymbol{x})$ is characterized by the implicit equation $\boldsymbol{x}^{\mathsf{T}} \boldsymbol{N}(\tau) \boldsymbol{x} = 0$. Therefore, we can simply apply the implicit function theorem, whose condition $(\phi_{\boldsymbol{x}}(s) = 0 \Rightarrow \dot{\phi}_{\boldsymbol{x}}(s) \neq 0)$ is satisfied by ours. □

Remark 1: The condition in Proposition 4 is equivalent, by the s-procedure, to the linear matrix inequality $\exists \lambda \in \mathbb{R} : \lambda \boldsymbol{N}(s) + \dot{\boldsymbol{N}}(s) \succ \boldsymbol{0}$. Note that it is trivially satisfied if $\dot{\boldsymbol{N}}(s) \succ \boldsymbol{0}$ for all $s \in [0, \bar{\tau}]$, which holds when the triggering function $\phi_{\boldsymbol{x}}$ is monotonically increasing for all $\boldsymbol{x}$.

The condition in Proposition 4 ensures that the triggering function crosses zero only once for each initial condition $\boldsymbol{x}$, which in turn simplifies the isochronous subset description to a simple quadratic form and renders f and τ continuous. As we will see, even when this continuity is observed, the behaviors generated by ETC can be extremely rich.

C. Problem Statement

We are interested in quantifying the traffic usage of system (1)–(3), which involves studying the sample system (7). Some candidate metrics are the following:

1) Inf $:= \inf_{\boldsymbol{x} \in \mathbb{R}^{n_x}} \tau(\boldsymbol{x})$;
2) Sup $:= \sup_{\boldsymbol{x} \in \mathbb{R}^{n_x}} \tau(\boldsymbol{x})$;
3) InfLimInf $:= \inf_{\boldsymbol{x} \in \mathbb{R}^{n_x}} \liminf_{i \to \infty} y_i(\boldsymbol{x})$;
4) SupLimSup $:= \sup_{\boldsymbol{x} \in \mathbb{R}^{n_x}} \limsup_{i \to \infty} y_i(\boldsymbol{x})$;
5) InfLimAvg $:= \inf_{\boldsymbol{x} \in \mathbb{R}^{n_x}} \liminf_{n \to \infty} \frac{1}{n+1} \sum_{i=0}^{n} y_i(\boldsymbol{x})$.
6) SupLimAvg $:= \sup_{\boldsymbol{x} \in \mathbb{R}^{n_x}} \limsup_{n \to \infty} \frac{1}{n+1} \sum_{i=0}^{n} y_i(\boldsymbol{x})$.

The first two metrics are simply the minimal and maximal interevent times that can be exhibited. The former has received most attention in the literature, mainly to prove absence of Zeno behavior. These metrics serve as worst- and best-case ISTs and provide basic information about how sample-efficient one given ETC system is. Inf is trivially calculated as Inf $= \inf\{s \in \mathcal{T} \mid \boldsymbol{N}(s) \not\succ \boldsymbol{0}\}$, while Sup is more involved: Sup $= \min(\bar{\tau}, \inf\{s \in \mathcal{T} \mid \forall \boldsymbol{x} \in \mathbb{R}^{n_x} \exists s' < s : \boldsymbol{x}^{\mathsf{T}} \boldsymbol{N}(s') \boldsymbol{x} > \boldsymbol{0}\})$. The last four metrics concern limit behaviors of the system. InfLimInf (SupLimSup) gives what is the minimal (maximal) IST the system can exhibit as the number of samples goes to infinity, i.e., after transients on the sequence $\{y_i\}$ vanish. Finally, InfLimAvg (SupLimAvg) gives the minimum (maximum), among initial states, average IST. Here, lim inf (lim sup) is used to ensure that the value exists even if the sequence of averages does not converge.

We argue that the limit metrics are more informative to determine the performance of a sampling mechanism than the simpler Inf and Sup metrics. For instance, if the states $\boldsymbol{x}$ associated to Inf are transient, the Inf metric turns out to be very conservative: after a few samples, the typical IST of the system will be higher. InfLimInf gives the complementary information of what minimal IST can appear infinitely often. InfLimAvg informs about the average utilization rate. A disadvantage of these two metrics is that they can still capture exceptional behavior: suppose, for example, that a measure-zero set $\mathcal{X} \subset \mathbb{R}^{n_x}$ is invariant under (7) and it is associated to the InfLimInf or InfLimAvg of the system; moreover, suppose for every state $\boldsymbol{x} \notin \mathcal{X}$, the trajectories $\boldsymbol{\xi}_{\boldsymbol{x}}(t_i), i \in \mathbb{N}$, never enter $\mathcal{X}$, but instead converge to some other subset with higher values of InfLimInf or InfLimAvg. Then, the metric will not reflect the dominant performance of the system. While this information might still be useful, a more robust version of these metrics is of interest.

All these observations lead to our main problem statement as follows:

Problem statement: Given an ETC system,

1) identify its limit traffic patterns;
2) characterize their robustness w.r.t. small perturbations in the initial state;
3) compute the system's robust limit metrics.

IV. Qualitative Analysis: Limit Behaviors in ETC

In this section, we investigate the limit behaviors of the traffic generated by ETC. We first see that limit metrics are insensitive to transient behavior; then we look at some examples to classify the different limit behaviors that can be exhibited. In several cases, ETC traffic converges to a periodic sampling pattern, which is shown to be characterized by linear invariants. This allows us to show that, if PETC stabilizes a periodic traffic pattern, then this traffic pattern can be used as a sampling schedule that guarantees GES of the system.

A. Properties of Limit Metrics

The following trivial result shows that limit metrics are insensitive to transient behavior. We focus on inferior metrics, as the superior counterparts follow similar reasoning.

Proposition 5: Let $\{k_i\}$ be a sequence of real numbers and decompose it as $k_i = a_i + b_i$, where b_i is the *transient component*, i.e., it satisfies $\lim_{i\to\infty} b_i = 0$. Then,

i) $\liminf_{i\to\infty} k_i = \liminf_{i\to\infty} a_i$;
ii) $\liminf_{n\to\infty} \frac{1}{n+1}\sum_{i=0}^{n} k_i = \liminf_{n\to\infty} \frac{1}{n+1}\sum_{i=0}^{n} a_i$.

Proof: It is a property of $\liminf$ that $\liminf_{i\to\infty}(a_i + b_i) = \liminf_{i\to\infty} a_i + \liminf_{i\to\infty} b_i$ if either $\{a_i\}$ or $\{b_i\}$ converge. Thus, result (i) trivially holds. For item (ii), we only need to prove that the sequence $\{\frac{1}{n+1}\sum_{i=0}^{n} b_i\}$ converges and is equal to zero. For this, we apply the Stolz–Cesàro theorem:

$$\liminf_{n\to\infty} b_i = 0 \le \liminf_{n\to\infty} \frac{1}{n+1}\sum_{i=0}^{n} b_i \le \limsup_{n\to\infty} b_i = 0$$

which concludes the proof. □

Corollary 1: Let $\{k_i\}$ be *ultimately periodic*, i.e., $k_i = a_i + b_i$, $\lim_{i\to\infty} b_i = 0$, and $a_{i+M} = a_i$ for some $M \in \mathbb{N}_+$ and all i. Then,

1) $\liminf_{i\to\infty} k_i = \min_{i<M} a_i$;
2) $\liminf_{n\to\infty} \frac{1}{n+1}\sum_{i=0}^{n} k_i = \frac{1}{M}\sum_{i=0}^{M-1} a_i$.

Proposition 5 implies that computing limit metrics of ETC is fundamentally a problem of finding its limit behaviors, ignoring transients. In particular, given Corollary 1, if a sequence of interevent times y_i converges to a periodic pattern, then the limit metrics are solely functions of the periodic component. This motivates us to study fixed and periodic solutions of (7); for example, if some y is a recurring pattern of (7), then there must be a subset of $\mathcal{Q}_y$ that is invariant. This is done in Section IV-C. Before that, we investigate some examples to understand what are the possible limit behaviors exhibited by ETC.

B. Illustrative Example

Consider system (1)–(3) with $n_x = 2$. In this case, an o-line is uniquely defined by the angle $\theta := \text{angle}(\boldsymbol{x}) := \arctan x_1/x_2 \in [-\pi/2, \pi/2)$. Using the coordinate θ and identifying points along an o-line (that is, regarding any point along an o-line as the same), the sample system (7) becomes

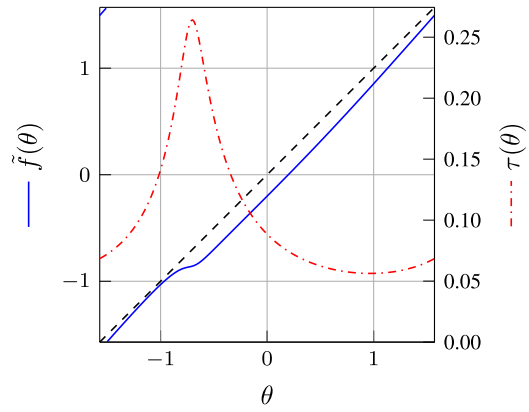

Fig. 1. Map $\tilde{f}$ and interevent time τ for case 1 of Example 1.

$$\theta_{i+1} = \tilde{f}(\theta_i) := \text{angle}\left(f\left(\begin{bmatrix}\sin\theta & \cos\theta\end{bmatrix}^{\mathsf{T}}\right)\right),$$
$$y_i = \tilde{\tau}(\theta) := \tau\left(\begin{bmatrix}\sin\theta & \cos\theta\end{bmatrix}^{\mathsf{T}}\right). \tag{8}$$

The map $\tilde{f}$ can be seen as a map on the circle. An analysis of system (8) has been conducted in [12], aiming at finding fixed points or their absence. In the cases studied therein, when $\tilde{f}$ had fixed points, it always had a stable one. In the next example, we show that this is not always true, and investigate the many possible behaviors that ETC traffic exhibits.

Example 1: Consider system (1)–(3) with

$$\boldsymbol{A} = \begin{bmatrix}0 & 1,\\ -2 & 3\end{bmatrix},\ \boldsymbol{B} = \begin{bmatrix}0\\1\end{bmatrix}$$
$$c(s, \boldsymbol{x}, \hat{\boldsymbol{x}}) = |\boldsymbol{x} - \hat{\boldsymbol{x}}| > a|\boldsymbol{x}| \tag{9}$$

where $a \in (0, 1)$ is the triggering parameter. This is the seminal triggering condition of [1], which can be put in the form (3) with sufficiently large $\bar{\tau}$. The graphs of $\tilde{f}$ and $\tau(\cdot)$, for CETC ($\mathcal{T} = \mathbb{R}_+$) are given for four cases.

1) $\boldsymbol{K} = [0 \quad -5], a = 0.2$: Fig. 1. This map is invertible, orientation-preserving,[5] and has no fixed points.
2) $\boldsymbol{K} = [0 \quad -6], a = 0.32$: Fig. 2(a). This map is no longer invertible. It has one unstable fixed point near $\theta = -1.3$ and one stable fixed point near $\theta = -0.6$.
3) $\boldsymbol{K} = [0 \quad -6, a = 0.5$: Fig. 2(b). This map has two unstable fixed points, but a stable period-4 solution as indicated by the cobweb diagram.
4) $\boldsymbol{K} = [0 \quad -6], a = 0.6$: Fig. 2(c). This map has no stable fixed points or orbits, and exhibits chaotic behavior. By inspection of the graph, the system has as a minimal set[6] the interval $[-1.07, -0.42]$, which contains the maximum IST $\bar{\tau} \approxeq 0.76$, so SupLimSup = Sup $\approxeq 0.76$.

Finally, notice that all these maps are differentiable, but this is not always the case, as has been observed in [12]. In particular, it is almost never the case for PETC ($\mathcal{T} = h\mathbb{N}$). One example is

[5] A map $f : \mathcal{X} \to \mathcal{X}$ is said to be *orientation-preserving* if its Jacobian J_f satisfies $\det(J_f(\boldsymbol{x})) > 0$ for all $\boldsymbol{x} \in \mathcal{X}$.

[6] A minimal set is an invariant set which contains no proper subsets that are also invariant.

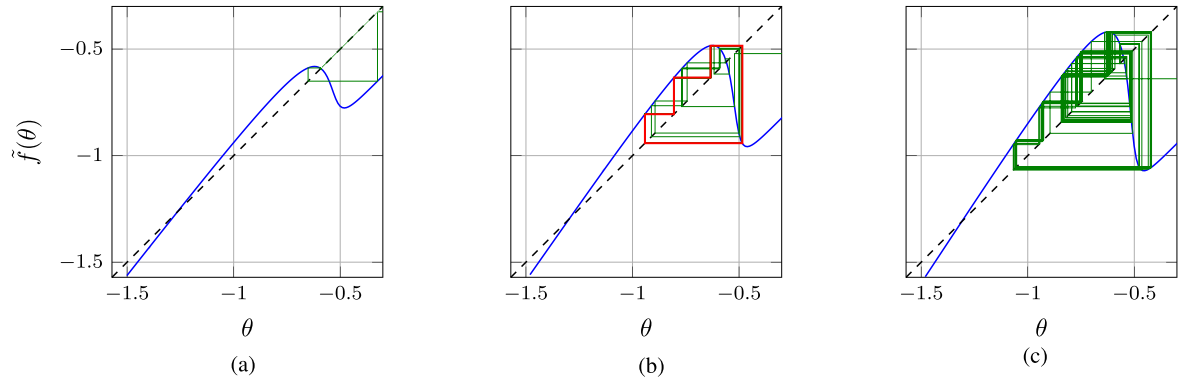

Fig. 2. Maps $\tilde{f}$ for Example 1, along with cobweb diagrams of solutions of (8) starting from $\theta_0 = 0$. A stable orbit for Case 3 is highlighted in red. (a) Case 2. (b) Case 3. (c) Case 4.

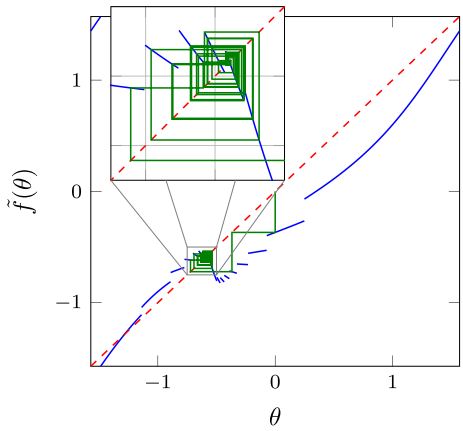

Fig. 3. Map $\tilde{f}$ of the PETC version of Example 1, case 2, with $h = 0.05$, and a cobweb diagram of a solution of (8) with $\theta_0 = 0$.

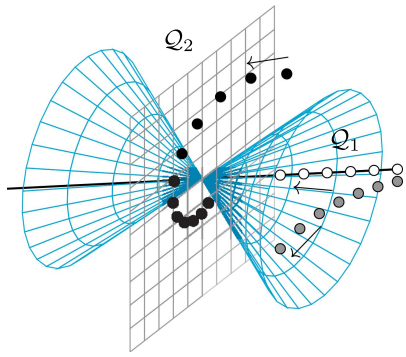

Fig. 4. Illustration of Theorem 2 in $\mathbb{R}^3$. The blue cone splits $\mathbb{R}^3$ into $\mathcal{Q}_1$ and $\mathcal{Q}_2$ the line is an invariant of $\boldsymbol{M}(1)$ and the plane is an invariant of $\boldsymbol{M}(2)$. Points indicate distinct sample trajectories $\{\boldsymbol{x}_i\}$, with the arrows indicating progress of time.

shown in Fig. 3, for $\boldsymbol{K} = [0 \quad -6], a = 0.32$ (like case 2) and $h = 0.05$. Different from the CETC case, its fixed points are unstable and it exhibits chaos.

Remark 2: Invertible orientation-preserving maps on the circle have been extensively studied in the field of dynamical systems [28], and they have an attribute called *rotation number*. When this number is a rational p/q, p and q coprime, all solutions converge to a q-periodic orbit. When it is irrational, all solutions are quasiperiodic: oscillatory, but the same point is never visited twice. In the latter case, if $\tilde{f}$ is twice continuously differentiable, it is topologically conjugate to an irrational rotation $g(\theta) = (\theta + r\pi \mod \pi) - \pi/2$, which is ergodic with dense orbit in $[-\pi/2, \pi/2)$. Hence, InfLimInf = Inf, and InfLimAvg = SupLimAvg can be obtained to arbitrary precision through simulations from any initial condition.

C. Invariant Isosequential Sets in ETC

Example 1 illustrates the complex behavior that can emerge in ETC traffic. Nonetheless it becomes apparent that obtaining fixed or periodic patterns is a fundamental step in the traffic characterization. The first thing we want is a computational or analytical method to determine fixed and periodic patterns. Then, we want to characterize their local stability.

In [23], it has been shown that periodic patterns can be characterized by linear invariants.

Theorem 2: (see [23]) Consider system (7), let $\sigma := y_1 y_2 \ldots y_m$ be a sequence of m outputs. Denote by $\boldsymbol{M}_\sigma := \boldsymbol{M}(y_m) \cdots \boldsymbol{M}(y_2)\boldsymbol{M}(y_1)$. (i) If $\boldsymbol{M}_\sigma$ is nonsingular and there exists a linear invariant $\mathcal{A}$ of $\boldsymbol{M}_\sigma$ such that $\mathcal{A} \setminus \{\boldsymbol{0}\} \subseteq \mathcal{Q}_\sigma$, then σ^ω is a possible output sequence of system (7). Moreover, if (ii) $\boldsymbol{M}_\sigma$ is additionally mixed and of irrational rotations, then σ^ω being an output sequence of system (7) implies that there exists a linear invariant $\mathcal{A}$ of $\boldsymbol{M}_\sigma$ such that $\mathcal{A} \subseteq \mathrm{cl}(\mathcal{Q}_\sigma)$.

According to Theorem 2, ETC exhibits a periodic sampling pattern whenever a linear invariant of the corresponding linear system is contained in the associated isosequential subset; in fact, the set $\mathcal{A} \setminus \{\boldsymbol{0}\}$ is a periodic set (with period m) of f. An illustration for a PETC system with $n_\mathrm{x} = 3$ and $\bar{k} = 2$ is given in Fig. 4: because an invariant of $\boldsymbol{M}(1)$ is a subset of $\mathcal{Q}_1$, we know that 1^ω is a sampling pattern exhibited by the system; likewise with $\boldsymbol{M}(2)$. The corollary given below (see the proof in the Appendix) states that in general this invariant is an o-line (or *o-plane*, a plane through the origin), and we have an if-and-only-if condition.

Corollary 2: Given the premises of Theorem 2, assume (i) $\boldsymbol{M}_\sigma$ is nonsingular, mixed, and of irrational rotations, and that (ii) for every linear invariant $\mathcal{A}$ of $\boldsymbol{M}_\sigma$, $\mathcal{A} \subseteq \mathrm{cl}(\mathcal{Q}_\sigma) \Rightarrow \mathcal{A} \setminus$

$\{\mathbf{0}\} \subseteq \mathcal{Q}_\sigma$. Then, σ^ω is a possible output sequence of system (7) if and only if there exists an o-line or o-plane $\mathcal{A}$ invariant of $\boldsymbol{M}_\sigma$ such that $\mathcal{A} \setminus \{\mathbf{0}\} \subseteq \mathcal{Q}_\sigma$.

Condition (ii) is satisfied in the illustrative example of Fig. 4, as the invariants lie in the interior of the corresponding isochronous sets. This result is particularly useful to verify whether a given periodic sequence is exhibited by system (7), and is instrumental in the symbolic methods used in Section V.

Remark 3: Using Corollary 2, one can find fixed inter-sample patterns $(t)^\omega$ by searching over $t \in [\underline{\tau}, \bar{\tau}]$ for an $\boldsymbol{M}(t)$ which has a linear subspace belonging to $\mathcal{Q}_t$ (via Proposition 1). This search is one-dimensional, in contrast to the search for invariants of system (7) over $\mathbb{R}^{n_\mathrm{x}}$.

The following lemma is useful when dealing with fixed o-lines.

Lemma 1: Let $\boldsymbol{l}$ be a fixed o-line of f in system (7), i.e., $\boldsymbol{x} \in \boldsymbol{l} \Rightarrow f(\boldsymbol{x}) \in \boldsymbol{l}$. Then, there exists a real λ such that $f(\boldsymbol{x}) = \lambda \boldsymbol{x}$ for all $\boldsymbol{x} \in \boldsymbol{l}$.

Proof: By Proposition 2, every $\boldsymbol{x} \in \boldsymbol{l}$ shares the same IST τ. Then, for any such $\boldsymbol{x}$, $f(\boldsymbol{x}) = \boldsymbol{M}(\tau)\boldsymbol{x} \in \boldsymbol{l}$; therefore, $f(\boldsymbol{x}) = \alpha(\boldsymbol{x})\boldsymbol{x}$ for some scalar-valued function α. By definition of eigenvalues, $\boldsymbol{x}$ is an eigenvector of $\boldsymbol{M}(\tau)$ and $\alpha(\boldsymbol{x}) \equiv \lambda$ is the corresponding eigenvalue. □

For some classic triggering conditions, we can get some interesting specialized results that relate the triggering parameter with the eigenvalues of the matrix $\boldsymbol{M}(\tau)$ for which τ is a periodic pattern:

Proposition 6: Consider system (1)–(3) with $c(s, \boldsymbol{x}, \hat{\boldsymbol{x}}) \equiv |\boldsymbol{x} - \hat{\boldsymbol{x}}| > a|\boldsymbol{x}|$, $\mathcal{T} = \mathbb{R}_+$, and assume $0 < a < 1$ is designed rendering the closed-loop system GES. A fixed o-line with IST τ exists iff $1/(1+a) \in \lambda(\boldsymbol{M}(\tau))$.

Proof: Consider a fixed o-line $\boldsymbol{l}$ and a trajectory $\boldsymbol{x}(t_i)$ on it. By Lemma 1, it holds that $\hat{\boldsymbol{x}}(t_{i+1}) = \lambda \hat{\boldsymbol{x}}(t_i)$, where λ is a real eigenvalue of $\boldsymbol{M}(\tau)$. Fix $\boldsymbol{z} := \hat{\boldsymbol{x}}(t_i)$. From the triggering condition, it then holds that $|\lambda \boldsymbol{z} - \boldsymbol{z}| = a|\lambda \boldsymbol{z}|$. Hence, $|\lambda - 1| = a|\lambda| \therefore \lambda = 1/(1 \pm a)$. Since $|\lambda| < 1$ for GES, $\lambda = 1/(1+a) < 1$. □

Proposition 7: Consider system (1)–(3) with $c(s, \boldsymbol{x}, \hat{\boldsymbol{x}}) \equiv \boldsymbol{x}^\mathsf{T}\boldsymbol{P}\boldsymbol{x} > \mathrm{e}^{-2\rho s}\hat{\boldsymbol{x}}^\mathsf{T}\boldsymbol{P}\hat{\boldsymbol{x}}$, $\mathcal{T} = \mathbb{R}_+$, with $0 < \rho < 1$ and $\boldsymbol{P} \succ \mathbf{0}$.[7] A fixed o-line with IST τ exists iff either $\mathrm{e}^{-\rho\tau}$ or $-\mathrm{e}^{-\rho\tau}$ is an eigenvalue of $\boldsymbol{M}(\tau)$.

Proof: Using the same arguments as in Proposition 6, we have that $\hat{\boldsymbol{x}}(t_{i+1}) = a\hat{\boldsymbol{x}}(t_i)$. Let $\boldsymbol{z} := \sqrt{\boldsymbol{P}}\hat{\boldsymbol{x}}(t_i)$. An invariant o-line then satisfies $a^2\boldsymbol{z}^\mathsf{T}\boldsymbol{z} = \mathrm{e}^{-2\rho\tau}\boldsymbol{z}^\mathsf{T}\boldsymbol{z} \therefore a = \pm\mathrm{e}^{-\rho\tau}$. Now, $\sqrt{\boldsymbol{P}}^{-1}\boldsymbol{M}(\tau)\sqrt{\boldsymbol{P}}\hat{\boldsymbol{x}} = \sqrt{\boldsymbol{P}}^{-1}\boldsymbol{M}(\tau)\boldsymbol{z} = a\sqrt{\boldsymbol{P}}^{-1}\boldsymbol{z} = a\hat{\boldsymbol{x}}$. Since $\boldsymbol{M}(\tau)$ is similar to $\sqrt{\boldsymbol{P}}^{-1}\boldsymbol{M}(\tau)\sqrt{\boldsymbol{P}}$, $a \in \lambda(\boldsymbol{M}(\tau))$. □

A more general result can be obtained by invoking a result from topology (see the proof in the Appendix) to conclude about which cases a fixed o-line certainly exists, only by knowing the state-space dimension n_x;

Theorem 3: Consider system (7) and assume f is continuous. If n_x is odd, then f has a fixed o-line.

Apart from o-lines, it is also interesting to know when can o-planes be fixed, as illustrated in the PETC example of Fig. 4. The next result presents for which dimensions this can generally hold (the proof is also in the Appendix).

Theorem 4: If system (7) exhibits a fixed o-plane $\mathcal{P}$ that is isochronous with some IST τ, then one of the following holds:

i) $n_\mathrm{x} = 2$ and $\underline{\tau} = \bar{\tau}$ (periodic sampling, trivial);
ii) $n_\mathrm{x} = 3$, and $\mathcal{T} = h\mathbb{N}$ (PETC) or $\boldsymbol{N}(\tau)$ is singular CETC;
iii) $n_\mathrm{x} \geq 4$.

D. Local Attractivity of Isochronous Invariants

After having determined the fixed (or periodic) o-lines and o-planes of system (7), the next step is to characterize their (local) attractivity. We say that an o-line $\boldsymbol{l} \subset \mathbb{R}^{n_\mathrm{x}}$ is attractive if for any other o-line $\boldsymbol{l}'$ s.t. the angle between $\boldsymbol{l}$ and $\boldsymbol{l}'$ is sufficiently small, $\lim_{n\to\infty} f^n(\boldsymbol{l}') = \boldsymbol{l}$. The following can be applied for fixed o-lines (see proof in the Appendix.)

Proposition 8: Let $\boldsymbol{l} := \{a\boldsymbol{x} \mid a \in \mathbb{R} \setminus \{0\}\}$ be a fixed o-line of system (7), and suppose f is differentiable at $\boldsymbol{x}$, with $J_f(\boldsymbol{x})$ being the corresponding Jacobian matrix. Take λ as the real s.t. $f(\boldsymbol{x}) = \lambda\boldsymbol{x}$ (Lemma 1), and let $\boldsymbol{O}_{\boldsymbol{x}}$ be an orthonormal basis for the orthogonal complement of $\boldsymbol{x}$. Then, if $\frac{1}{\lambda}\boldsymbol{O}_{\boldsymbol{x}}{}^\mathsf{T} J_f(\boldsymbol{x})\boldsymbol{O}_{\boldsymbol{x}}$ is Schur, then $\boldsymbol{l}$ is locally attractive.

The Jacobian matrix can be expressed as $J_f = \partial(\boldsymbol{M}(\tau(\boldsymbol{x}))\boldsymbol{x})/\partial\boldsymbol{x} = \partial(\boldsymbol{M}(\tau(\boldsymbol{x}))/\partial\boldsymbol{x})\boldsymbol{x} + \boldsymbol{M}(\tau(\boldsymbol{x})) =$

$$\frac{-2}{\boldsymbol{x}^\mathsf{T}\dot{\boldsymbol{N}}(\tau(\boldsymbol{x}))\boldsymbol{x}}\dot{\boldsymbol{M}}(\tau(\boldsymbol{x}))\boldsymbol{x}\boldsymbol{x}^\mathsf{T}\boldsymbol{N}(\tau(\boldsymbol{x})) + \boldsymbol{M}(\tau(\boldsymbol{x})). \quad (10)$$

The matrix $\boldsymbol{O}_{\boldsymbol{x}}{}^\mathsf{T} J_f(\boldsymbol{x})\boldsymbol{O}_{\boldsymbol{x}}$ is the Jacobian of f w.r.t. the non-radial directions and projected onto those. It is easy to see that the eigenvalues of $\boldsymbol{O}_{\boldsymbol{x}}{}^\mathsf{T} J_f(\boldsymbol{x})\boldsymbol{O}_{\boldsymbol{x}}$ are the same as those of J_f except the one associated with the eigenvector $\boldsymbol{x}$, while λ is precisely the eigenvalue associated with $\boldsymbol{x}$; hence, Proposition 8 gives a condition on the ratio between the largest-in-magnitude eigenvalue of J_f and that of the fixed o-line in consideration. For fixed planes, this analysis may require more sophisticated analyses of orbital stability, such as Poincaré return maps.

As we see next, the case of PETC is revealing thanks to the fact that $\boldsymbol{M}$ is constant by parts and, thus, $J_f = \boldsymbol{M}(\tau(\boldsymbol{x}))$ almost everywhere. Because PETC has a discrete output set, we must first properly define stability of an infinite sequence.

Definition 8: Consider system (7) with $\mathcal{T} = h\mathbb{N}$ (PETC). An infinite sequence of outputs $\{y_i\}$ is said to be stable if there exists $\boldsymbol{x} \in \mathbb{R}^{n_\mathrm{x}}$ with a neighborhood $\mathcal{U}$ such that every $\boldsymbol{x}' \in \mathcal{U}$ satisfies $y_i(\boldsymbol{x}') = y_i(\boldsymbol{x}) = y_i, \forall i \in \mathbb{N}$.

Proposition 9: Consider system (7) with $\mathcal{T} = h\mathbb{N}$ (PETC) and assume it is GES. Let $\{y_i\}$ be a p-periodic output trajectory associated with it, and let $\boldsymbol{M} := \boldsymbol{M}(y_{p-1}) \cdots \boldsymbol{M}(y_1)\boldsymbol{M}(y_0)$. If $\{y_i\}$ is stable, then $\boldsymbol{M}$ is Schur.

Proof: Every trajectory $\{\boldsymbol{x}_i\}$ of (7) that generates $\{y_i\}$ satisfies $\boldsymbol{x}_{i+p} = \boldsymbol{M}\boldsymbol{x}_i$. If $\boldsymbol{M}$ is not Schur, then from almost every $\boldsymbol{x}_0$, (and hence for any point's neighborhood) there are no $M > 0, 0 < a < 1$ such that $|\boldsymbol{x}_{mp}| \leq Ma^m|\boldsymbol{x}_0|$, which implies that the PETC system is not GES. This is a contradiction. □

Proposition 9 implies that stable fixed or periodic sampling patterns generated by a PETC system can be used in a multirate periodically sampled system that also renders the origin GES. Note that the existence of such a stable periodic sampling pattern does not imply that the PETC generates that pattern everywhere;in fact, it may generate sequences that converge to this stable sequence. In these cases, the PETC has a rival periodic sampling schedule which also achieves

[7] This is the triggering condition initially used for STC in [27].

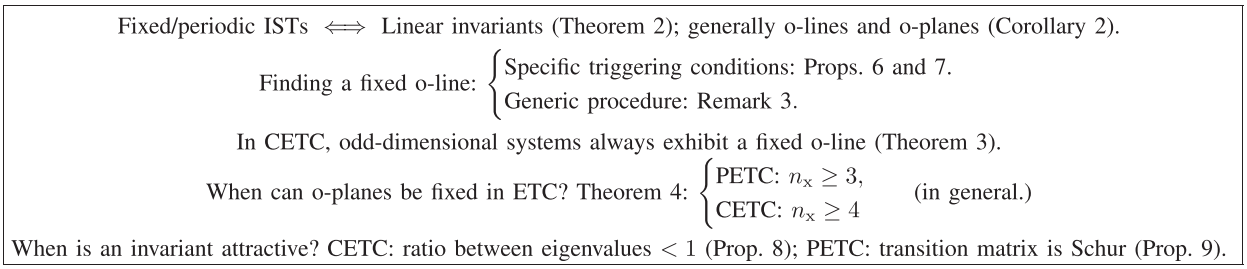

Fig. 5. Informal summary of the results in Section IV.

GES.[8] This is not necessarily true if no stable periodic pattern is exhibited, i.e., when PETC exhibits chaotic or aperiodic traffic.

Remark 4: Proposition 9 and its associated conclusion are not true for CETC. For example, consider the case 2 from Ex. 1: its stable fixed point occurs for the interevent time $y \approx 0.3903$; the eigenvalues of $\boldsymbol{M}(y)$ are 0.757 (which is $1/(1+\sigma)$ as expected from Proposition 6) and -1.33, hence $\boldsymbol{M}(y)$ is not Schur. Given Proposition 9, it is now not surprising that case 2's PETC implementation (see Fig. 3) does not exhibit an asymptotically stable interevent time trajectory. More interestingly, this stays true regardless of how small h is.

This section has presented many properties of fixed and periodic subsets of ETC, such as dimensional conditions for fixed o-lines and o-planes to exist, how to find them, and how to characterize their attractivity, which we summarize in Fig. 5. However, it has not yet provided a means to compute the limit metrics or their robust versions. Looking again at Example 1, it is clear that several challenges remain.

1) If a stable fixed or periodic pattern is found, can we ensure that it is almost globally attractive? (Here, almost is used to exclude the finitely many unstable fixed or periodic patterns, in case these exist.)
2) If f has fixed or periodic patterns, how can we obtain some information about the limit metrics?
3) If multiple fixed or periodic patterns are found, but inside a chaotic invariant set, how to compute robust limit metrics?

The following section provides (partial) answers to these questions for PETC using a symbolic approach.

V. Quantitative Analysis: A Symbolic Approach

In this section, we shift from the nonlinear analysis tools used in Section IV to symbolic tools in the spirit of [14]. We focus on PETC, whose discrete-output nature facilitates the construction of finite-state models [18]. For this part, it is necessary to introduce some formalism and previous results.

A. Transition Systems, Simulations, and Quantitative Automata

Tabuada [14] gives a generalized notion of transition system.

Definition 9 (Transition System [14]): A system $\mathcal{S}$ is a tuple $(\mathcal{X}, \mathcal{X}_0, \mathcal{E}, \mathcal{Y}, H)$ where:

- $\mathcal{X}$ is the set of states;
- $\mathcal{X}_0 \subseteq \mathcal{X}$ is the set of initial states;
- $\mathcal{E} \subseteq \mathcal{X} \times \mathcal{X}$ is the set of edges (or transitions);
- $\mathcal{Y}$ is the set of outputs;
- $H : \mathcal{X} \to \mathcal{Y}$ is the output map.

Here, we have omitted the action set $\mathcal{U}$ from the original definition because we focus on autonomous systems. A system is said to be finite (infinite) state when the cardinality of $\mathcal{X}$ is finite (infinite). A transition in $\mathcal{E}$ is denoted by a pair (x, x'). We define $\mathrm{Post}_{\mathcal{S}}(x) := \{x' \mid (x, x') \in \mathcal{E}\}$ as the set of states that can be reached from x in one step. System $\mathcal{S}$ is said to be *nonblocking* if $\forall x \in \mathcal{X}, \mathrm{Post}_{\mathcal{S}}(x) \neq \emptyset$. We call $x_0 x_1 x_2 \ldots$ an *infinite internal behavior*, or *run* of $\mathcal{S}$ if $x_0 \in \mathcal{X}_0$ and $(x_i, x_{i+1}) \in \mathcal{E}$ for all $i \in \mathbb{N}$, and $y_0 y_1 \ldots$ its corresponding *infinite external behavior*, or *trace*, if $H(x_i) = y_i$ for all $i \in \mathbb{N}$. We denote by $B_{\mathcal{S}}(r)$ the external behavior from a run $r = x_0 x_1 \ldots$ (in the case above, $B_{\mathcal{S}}(r) = y_0 y_1 \ldots$), by $\mathcal{B}^l_x(\mathcal{S})$ (resp. $\mathcal{B}^+_x(\mathcal{S})$ and $\mathcal{B}^\omega_x(\mathcal{S})$) the set of all l-long (resp. finite and infinite) external behaviors of $\mathcal{S}$ starting from state x, and by $\mathcal{B}^l(\mathcal{S}) := \bigcup_{x \in \mathcal{X}_0} \mathcal{B}^l_x(\mathcal{S})$ (resp. $\mathcal{B}^+(\mathcal{S}) := \bigcup_{x \in \mathcal{X}_0} \mathcal{B}^+_x(\mathcal{S})$ and $\mathcal{B}^\omega(\mathcal{S}) := \bigcup_{x \in \mathcal{X}_0} \mathcal{B}^\omega_x(\mathcal{S})$) the set of all l-long (resp. finite and infinite) external behaviors of $\mathcal{S}$.

The concepts of simulation and bisimulation are fundamental to establish formal relations between systems.

Definition 10 (Simulation Relation [14]): Consider two systems $\mathcal{S}_a$ and $\mathcal{S}_b$ with $\mathcal{Y}_a = \mathcal{Y}_b$. A relation $\mathcal{R} \subseteq \mathcal{X}_a \times \mathcal{X}_b$ is a simulation relation from $\mathcal{S}_a$ to $\mathcal{S}_b$ if the following conditions are satisfied:

i) for every $x_{a0} \in \mathcal{X}_{a0}$, there exists $x_{b0} \in \mathcal{X}_{b0}$ with $(x_{a0}, x_{b0}) \in \mathcal{R}$;
ii) for every $(x_a, x_b) \in \mathcal{R}, H_a(x_a) = H_b(x_b)$;
iii) for every $(x_a, x_b) \in \mathcal{R}$, we have that $(x_a, x'_a) \in \mathcal{E}_a$ implies the existence of $(x_b, x'_b) \in \mathcal{E}_b$ s.t. $(x_a, ' x'_b) \in \mathcal{R}$.

We say $\mathcal{S}_a \preceq \mathcal{S}_b$ when $\mathcal{S}_b$ simulates $\mathcal{S}_a$, which is true if there exists a simulation relation from $\mathcal{S}_a$ to $\mathcal{S}_b$. When $\mathcal{R}$ is a simulation relation from $\mathcal{S}_a$ to $\mathcal{S}_b$ and also $\mathcal{R}^{-1}$ is from $\mathcal{S}_b$ to $\mathcal{S}_a$, we say that $\mathcal{S}_a$ and $\mathcal{S}_b$ are *bisimilar*, and denote by $\mathcal{S}_a \cong \mathcal{S}_b$. Weaker but relevant relations associated with simulation and bisimulation are, respectively, *behavioral inclusion* and *behavioral equivalence.*

Definition 11 (Behavioral inclusion and equivalence [14]): Consider two systems $\mathcal{S}_a$ and $\mathcal{S}_b$ with $\mathcal{Y}_a = \mathcal{Y}_b$. We say that $\mathcal{S}_a$ is *behaviorally included* in $\mathcal{S}_b$, denoted by $\mathcal{S}_a \preceq_{\mathcal{B}} \mathcal{S}_b$, if $\mathcal{B}^\omega(\mathcal{S}_a) \subseteq \mathcal{B}^\omega(\mathcal{S}_b)$. In case $\mathcal{B}^\omega(\mathcal{S}_a) = \mathcal{B}^\omega(\mathcal{S}_b)$, we say that $\mathcal{S}_a$ and $\mathcal{S}_b$ are *behaviorally equivalent*, denoted by $\mathcal{S}_a \cong_{\mathcal{B}} \mathcal{S}_b$.

(Bi)simulations lead to behavioral inclusion (equivalence).

Theorem 5 (see [14]): Given two systems $\mathcal{S}_a$ and $\mathcal{S}_b$,$\mathcal{S}_a \preceq \mathcal{S}_b \Rightarrow \mathcal{S}_a \preceq_{\mathcal{B}} \mathcal{S}_b$ and $\mathcal{S}_a \cong \mathcal{S}_b \Rightarrow \mathcal{S}_a \cong_{\mathcal{B}} \mathcal{S}_b$.

[8] While both approaches stabilize the system with equal limit average sampling performances, their transients should be different; thus, their control performances can differ.

If $\mathcal{S}$ is finite-state, we can associate a digraph G with it, where states are nodes and an edge $x \to x'$ exists iff $(x, x') \in \mathcal{E}$. A digraph has an associated incidence matrix $\boldsymbol{T}$, obtained by attributing an index to each node, then $T_{ij} = 1$ if $x_i \to x_j$, $T_{ij} = 0$ otherwise. We call $\boldsymbol{T}$ the incidence matrix of $\mathcal{S}$.

For quantitative analysis of system properties, we resort to the framework of [24], with the adaptations made in [22] to include output maps.

Definition 12 (Weighted transition system (WTS) [22]): A WTS $\mathcal{S}$ is the tuple $(\mathcal{X}, \mathcal{X}_0, \mathcal{E}, \mathcal{Y}, H, \gamma)$, where

1) $(\mathcal{X}, \mathcal{X}_0, \mathcal{E}, \mathcal{Y}, H)$ is a *nonblocking* transition system;
2) $\gamma : \mathcal{E} \to \mathbb{Q}$ is the *weight function*.

For a given run $r = x_0 x_1 \dots$ of $\mathcal{S}$, abusing notation, $\gamma(r) = v_0 v_1 \dots$ is the sequence of weights defined by $v_i = \gamma(x_i, x_{i+1})$. We use $\gamma_i(r)$ for the ith element of $\gamma(r)$. A WTS is called *simple* if for all $(x, x') \in \mathcal{E}, \gamma(x, x') = H(x)$ [23]; in this case $\gamma(r) = B_{\mathcal{S}}(r)$, i.e., the set of weight sequences of $\mathcal{S}$ is equal to its behavior. All WTSs we consider in this work are simple, so hereafter we focus on this case. In this case, we define the following *values* of a behavior set $\mathcal{B} \subseteq 2^{\mathbb{N} \to \mathbb{Q}}$, in the spirit of the metrics presented in Section III-C:

$$\mathrm{ILI}(\mathcal{B}) := \inf \left\{ \liminf_{i \to \infty} y_i \mid \{y_i\} \in \mathcal{B} \right\},$$

$$\mathrm{ILA}(\mathcal{B}) := \inf \left\{ \liminf_{n \to \infty} \frac{1}{n+1} \sum_{i=0}^{n} y_i \;\middle|\; \{y_i\} \in \mathcal{B} \right\}.$$

For a value $V \in \{\mathrm{ILI}, \mathrm{ILA}\}$, we often use the shorthand notation $V(\mathcal{S}) := V(\mathcal{B}^\omega(\mathcal{S}))$. The following result is extracted from [23, Th. 3] and its proof.

Theorem 6: Given a finite-state WTS $\mathcal{S}$,

1) $\mathrm{ILI}(\mathcal{S})$ can be computed in $\mathcal{O}(|\mathcal{X}| + |\mathcal{E}|)$; moreover, there exists $x \in \mathcal{X}$ such that $H(x) = \mathrm{ILI}(\mathcal{S})$ and x belongs to a strongly connected component (SCC) of the graph defined by $\mathcal{S}$.
2) $\mathrm{ILA}(\mathcal{S})$ can be computed in $\mathcal{O}(|\mathcal{X}||\mathcal{E}|)$. Moreover, system $\mathcal{S}$ admits a cycle $x_0 x_1 \dots x_k$ satisfying $x_i \to x_{i+1}, i < k$, and $x_k \to x_0$, s.t. the run $r = (x_0 x_1 \dots x_k)^\omega$ satisfies $\liminf_{n \to \infty} \frac{1}{n+1} \sum_{i=0}^{n} \gamma_i(r)) = \mathrm{ILA}(\mathcal{S})$.

Theorem 6 gives that global values of limit metrics are *computable* for finite-state systems. This is fundamentally different from the infinite-state case, where a qualitative analysis is possible, but it is extremely challenging to determine regions of attraction of fixed lines, or computing tight bounds on the metrics when no fixed (periodic) solutions are found.

Remark 5: The algorithm for computing $\mathrm{ILI}(\mathcal{S})$ and $\mathrm{SLS}(\mathcal{S})$ is the same as the one to determine Büchi acceptance, and consists of computing SCCs and performing reachability to those [24]. The cycle mentioned in Theorem 6 is a *minimum average cycle* (MAC) of the weighted digraph defined by $\mathcal{S}$. The algorithm to compute the value is due to [29], which also detects reachable SCCs and employs dynamic programming on those. The cycle can be recovered in $\mathcal{O}(|\mathcal{X}|)$ using the algorithm in [30].

Remark 6: In case $\mathcal{S}$ is infinite, a method to compute $\mathrm{ILA}(\mathcal{S})$ using abstractions was proposed in [22], [23], and the same results can be extended to ILI. The main idea is to compute the metric on the abstraction and retrieve a cycle σ that attains the minimum value (an MAC when computing ILA or any cycle in the SCC that attains the ILI). The value of the abstraction is a lower bound to the value of the concrete system [23]. Then, one verifies if $\sigma^\omega \in \mathcal{B}^\omega(\mathcal{S})$ (in the PETC case, by using Theorem 2 with Proposition 1): if true, then the value of the abstraction is in fact *equal* to the value of the concrete system [22]; if not, one can refine the abstraction and reiterate. The following section presents how to abstract a PETC traffic model and refine it.

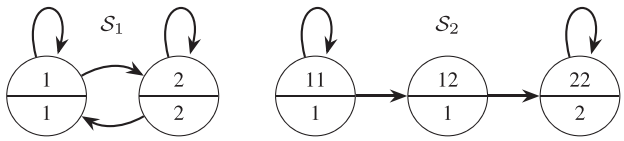

Fig. 6. l-complete models of the illustrative PETC system of Fig. 4, for $l = 1$ (left) and $l = 2$ (right). Each node represents a state, with the top label being the state label and the bottom being its output.

B. l-Complete PETC Traffic Models

Here, we recover results of our previous work [21], [22], which determines how to build a *finite-state system* that captures sequences of l ISTs from system (7) with $\mathcal{T} = h\mathbb{N}$ (PETC) and their associated state-space partition. First, let us describe the system (7) as a transition system

$$\begin{aligned} &\mathcal{S} = (\mathbb{R}^{n_x}, \mathbb{R}^{n_x}, \mathcal{E}, \mathcal{Y}, H, \gamma), \text{ where} \\ &\mathcal{E} = \{(\boldsymbol{x}, \boldsymbol{x}') \in \mathbb{R}^n \times \mathbb{R}^n \mid \boldsymbol{x}' = \boldsymbol{M}(\tau(\boldsymbol{x}))\boldsymbol{x}\}, \\ &\mathcal{Y} = \{h, 2h, \dots, \bar{\tau}\}, \\ &H(\boldsymbol{x}) = \gamma(\boldsymbol{x}, \boldsymbol{x}') = \tau(\boldsymbol{x}). \end{aligned} \tag{11}$$

Denote by $\mathcal{K} := \mathcal{Y}/h$, the set of possible interevent times normalized by h.

Definition 13 (see [22]): Given an integer $l \geq 1$, the *l-complete PETC traffic model* of system $\mathcal{S}$ from (11) is the system $\mathcal{S}_l := (\mathcal{X}_l, \mathcal{X}_l, \mathcal{E}_l, \mathcal{Y}, H_l, \gamma_l)$, with

1) $\mathcal{X}_l := \mathcal{B}^l(\mathcal{S})$;
2) $\mathcal{E}_l = \{(k\sigma, \sigma k') \mid k, k' \in \mathcal{K}, \sigma \in \mathcal{K}^{l-1}, k\sigma, \sigma k' \in \mathcal{X}_l\}$;
3) $H_l(k_1 k_2 \dots k_m) = \gamma_l(k_1 k_2 \dots k_m, \cdot) = h k_1$.

The state space of the model above is the set of l-long outputs that the PETC system $\mathcal{S}$ can generate, which can be computed by using the techniques described in [22]. The output of a state x is its next IST (divided by h), which is also the weight of any transition leaving x. The transition relation is what is called in [31] the domino rule: a state associated with a sequence $k_1 k_2 \dots k_l$ must lead to a state whose next first $l-1$ samples are $k_2 k_3 \dots k_l$, because the system is deterministic, autonomous, and time-invariant. Hence, any state in $\mathcal{X}_l$ that starts with $k_2 k_3 \dots k_l$ is a possible successor of $k_1 k_2 \dots k_l$. Note that both $\mathcal{S}$ and $\mathcal{S}_l$ are simple WTSs. The following result gives the desired simulation refinement properties.

Proposition 10 (see [22]): Consider the system $\mathcal{S}$ from (11) and $\mathcal{S}_l$ from Def. 13, for some $l \geq 1$. Then, $\mathcal{S} \preceq \mathcal{S}_{l+1} \preceq \mathcal{S}_l$, which implies that $\mathcal{S} \preceq_{\mathcal{B}} \mathcal{S}_{l+1} \preceq_{\mathcal{B}} \mathcal{S}_l$.

Fig. 6 shows l-complete models $\mathcal{S}_1$ and $\mathcal{S}_2$ for the illustrative PETC example of Fig. 4. For $l = 1$, it is simply the complete graph with states 1 and 2, corresponding to the possible ISTs the system exhibits. With $l = 2$, one needs sequences of length 2: in this illustrative case, it is verified (e.g., through [22]) that $\mathcal{X}_2 = \{(1,1), (1,2), (2,2)\}$; the transitions and outputs

are thus obtained using Def. 13. Note that $(1,2) \in \mathcal{X}_2$ means that there are points in $\mathbb{R}^3$ that belong to $\mathcal{Q}_1$, but the next sample would belong to $\mathcal{Q}_2$; at the same time, $(2,1) \notin \mathcal{X}_2$, which implies that no points leave $\mathcal{Q}_2$ after sampling, i.e., $\mathcal{Q}_2$ is forward-invariant. This kind of observation is central when using abstractions to differentiate robust from fragile behaviors.

C. Robust Limit Metrics

Limit metrics of PETC traffic can be computed using abstractions as described in Remark 6. However, as discussed in Section III-C, these metrics can be rare in the sense that they only occur from a zero-measure initial set, e.g., revisiting cases 2 and 3 of Example 1, we have 1 and 2 unstable fixed points, respectively. In both cases, the unstable fixed point near $\theta = -1.3$ gives the value of InfLimInf and InfLimAvg; but for all other initial conditions θ_0, trajectories $\{\theta_i\}$ are attracted to the stable fixed point in case 2 and the stable period-4 orbit in case 3. Thus, *robust limit metrics should be oblivious to unstable orbits.* Let us properly define what stable and unstable behaviors are for systems with a finite output set.

Definition 14 (Stable behaviors): Consider a deterministic WTS $\mathcal{S}$ where $\mathcal{X}$ is a metric space and $\mathcal{Y}$ is finite. A periodic behavior $\sigma^\omega \in \mathcal{B}^\omega(\mathcal{S})$ is said to be *stable* if there exists $x \in \mathcal{X}$ with a neighborhood $\mathcal{U}$ such that every $x' \in \mathcal{U}$ satisfies $\mathcal{B}^\omega_x = \mathcal{B}^\omega_{x'} = \sigma^\omega$ (as in Def. 8).

Definition 15 (Robust limit metrics): Let $\mathcal{S}$ be a simple WTS, $\mathcal{B}^\omega_{\mathrm{u}}(\mathcal{S})$ be the set of its unstable behaviors, and V be a system limit metric (ILA or ILI). Then, the robust version of the metric is $\mathrm{Rob}V(\mathcal{S}) := V(\mathcal{B}^\omega(\mathcal{S}) \setminus \mathcal{B}^\omega_{\mathrm{u}}(\mathcal{S}))$.

Removing unstable behaviors as the ones discussed above is safe in that small perturbations in the initial state lead to distant behaviors. However, consider case 4 of Example 1 and its chaotic invariant set: it has infinitely many unstable orbits, and almost every orbit comes arbitrarily close to those orbits. In fact, due to transitivity, *every initial solution starting on the chaotic invariant set will come arbitrarily close to any unstable orbit within it.* Thus, the infimum of a set of metrics on behaviors on a chaotic set, even when excluding the unstable ones, can be equal to one of its unstable behaviors. This deserves a further distinction between unstable behaviors.

Definition 16 (Absolutely unstable behaviors): Consider a deterministic WTS $\mathcal{S}$ where $\mathcal{X}$ is a metric space and $\mathcal{Y}$ is finite. A periodic behavior $\sigma^\omega \in \mathcal{B}^\omega(\mathcal{S})$ is said to be *absolutely unstable* (a.u.) if it is unstable and for almost all x there exists $L \in \mathbb{N}$ such that $\forall l > L$, σ^l is not a subsequence of $\mathcal{B}^\omega_x(\mathcal{S})$. The set of a.u. behaviors of $\mathcal{S}$ is denoted by $\mathcal{B}^\omega_{\mathrm{au}}(\mathcal{S})$.

A.u. behaviors are fragile in the sense that small perturbations to initial states lead to substantially different behaviors.

Periodic behaviors of a PETC system $\mathcal{S}$ that occur in an abstraction $\mathcal{S}_l$ can be verified to be (absolutely) unstable (see proof in the Appendix).

Proposition 11: Consider system $\mathcal{S}$ from (11) and let $\sigma^\omega \in \mathcal{B}^\omega(\mathcal{S})$. Assume $\boldsymbol{M}_k$ is nonsingular for all $k \in \{1,\dots,\bar{k}\}$. Furthermore, assume $\boldsymbol{M}_\sigma$ is mixed, and let $\boldsymbol{v}_1, \boldsymbol{v}_2, \dots, \boldsymbol{v}_n$ be the unitary eigenvectors of $\boldsymbol{M}$ ordered from largest-in-magnitude corresponding eigenvalue to smallest. Denote by $\mathcal{A}$ any linear invariant of $\boldsymbol{M}_\sigma$ containing $\boldsymbol{v}_1$. (I) If $\mathcal{A} \nsubseteq \mathrm{cl}(\mathcal{Q}_\sigma)$, then σ^ω is an unstable behavior. (II) If additionally the cycle $x_1x_2\dots x_c$ in $\mathcal{S}_l$ that generates σ^ω (i.e., $B_{\mathcal{S}_l}(\{x_1x_2\dots x_c\}^\omega) = \sigma^\omega$) is the only cycle of its SCC, then σ^ω is absolutely unstable in $\mathcal{S}$.

Hereafter, we shall denote a linear invariant $\mathcal{A}$ containing $\boldsymbol{v}_1$ as in Proposition 11 a *dominant* linear invariant, after the concept of dominant modes in linear systems. Referring again to Fig. 4 and the corresponding 2-complete model (see Fig. 6), we see two periodic behaviors, 1^ω and 2^ω. The illustrated o-line is an invariant of $\boldsymbol{M}(1)$ that is not dominant (as can be inferred by the trajectory of gray points that diverge from the line); moreover, the cycle of $\mathcal{S}_2$ that generates 1^ω is a simple cycle, the node 11 with a self loop. This implies that 1^ω is absolutely unstable. Note that this conclusion could not be obtained by inspecting $\mathcal{S}_1$, which is a complete graph without simple cycles. The behavior 2^ω, on the other hand, is stable.

Clearly, removing only a.u. behaviors is safe to give a lower bound estimate to $\mathrm{Rob}V(\mathcal{S})$, i.e., $V(\mathcal{B}^\omega(\mathcal{S}) \setminus \mathcal{B}^\omega_{\mathrm{au}}(\mathcal{S})) \leq V(\mathcal{B}^\omega(\mathcal{S}) \setminus \mathcal{B}^\omega_{\mathrm{u}}(\mathcal{S}))$. An equality holds when $\mathcal{S}$ is not chaotic, since all unstable behaviors are also absolutely unstable. Therefore, determining when $\mathcal{S}$ is or is not chaotic is critical to compute the exact value of $\mathrm{Rob}V(\mathcal{S})$. As we see next, chaos on $\mathcal{S}$ can be estimated from the abstraction $\mathcal{S}_l$.

D. Estimating Chaos in Abstractions

In this section, we show how to detect (and quantify) chaos on a PETC traffic model $\mathcal{S}$, and when one can conclude that $\mathcal{S}$ is not chaotic. A commonly used measure of chaos is the topological entropy $h(\mathcal{S}) \geq 0$ [25], with $h(\mathcal{S}) = 0$ implying there is no chaos. However, instead of a topological measure, we are interested in a measure of chaos of the output of the system: if the state is behaving chaotically but this is not reflected in the output, it does not interfere in our metrics of interest. Therefore, we introduce a notion called *behavioral entropy*, a natural extension of the original concept.

Definition 17 (Behavioral entropy): Consider a system $\mathcal{S}$ and equip $\mathcal{Y}$ with a metric d. A set $\mathcal{W} \subset \mathcal{B}^\omega(\mathcal{S})$ is called (n,ϵ)-separated if for all behaviors $\boldsymbol{y}, \boldsymbol{y}' \in \mathcal{W}$, where $\boldsymbol{y} = y_0y_1\dots y_i\dots$ and $\boldsymbol{y}' = y'_0y'_1\dots y'_i\dots$, we have $d(y_i, y'_i) > \epsilon$ for all $i \leq n$. Let $s(n,\epsilon,\mathcal{S})$ be the maximum cardinality of any (n,ϵ)-separated set. The behavioral entropy is the quantity

$$h(\mathcal{S}) := \lim_{\epsilon \to 0} \limsup_{n\to\infty} \frac{\log(s(n,\epsilon,\mathcal{S}))}{n}. \tag{12}$$

In particular, if $|\mathcal{Y}| < \infty$ and the distance metric is $d(y,y') = 0$ if $y = y'$ and $d(y,y') = 1$ otherwise, we can ignore the ϵ component, and it turns out that

$$h(\mathcal{S}) = \limsup_{n\to\infty} \frac{\log(N(n,\mathcal{S}))}{n}, \tag{13}$$

where $N(n,\mathcal{S})$ is the number of different words of length n over the alphabet $\mathcal{Y}$ that are possible trace segments of $\mathcal{S}$.

A system is called *behaviorally chaotic* whenever its behavioral entropy is positive.

Remark 7: The topological entropy also takes the form in (13) for *subshifts of finite type*, an abstraction used for autonomous dynamical systems to study their topological properties (see [25]).

Definition 17 takes a behavioral approach [32] to extend the original definition [25] for systems that are possibly nondeterministic and have output maps. If $H = \mathrm{Id}$ and $\mathrm{Post}(x) = \{f(x)\}$ for some continuous map $f : \mathcal{X} \to \mathcal{X}$, we recover the original notion. It may seem unproductive to extend a measure of chaos to nondeterministic systems, as these should all be chaotic in some sense; however, this is not always the case. For example,

consider $\mathcal{S}_2$ of Fig. 6: it is easy to see that $N(n,\mathcal{S}_2) = n+1: 11\ldots11, 11\ldots12, \ldots, 122\ldots22, 22\ldots22$. Hence, $h(\mathcal{S}_2) = \lim_{n\to\infty}(\log(n+1)/n) = 0$, and this system is not (behaviorally) chaotic.

The following result establishes that the behavioral entropy of an abstraction bounds that of the concrete system.

Proposition 12: Consider transition systems $\mathcal{S}_a$ and $\mathcal{S}_b$ with $\mathcal{Y}_a = \mathcal{Y}_b = \mathcal{Y}$ s.t. $\mathcal{S}_a \preceq_{\mathcal{B}} \mathcal{S}_b$. If $|\mathcal{Y}| < \infty$, then $h(\mathcal{S}_a) \leq h(\mathcal{S}_b)$.

Proof: Trivially, from behavioral inclusion [14], $\forall n \in \mathbb{N}, N(n,\mathcal{S}_a) \leq N(n,\mathcal{S}_b)$. The result follows from monotonicity of the log function. □

The question now is how to compute the behavioral entropy of a finite-state system. This result is known for topological entropy of subshifts of finite type, which is the same as a finite-state transition system with $H = \mathrm{Id}$.

Theorem 7 (see [25, Th. IX.1.9]):[9] Let $\mathcal{S}$ be a finite system and $N'(n,\mathcal{S})$ be the number of different n-long words over the alphabet $\mathcal{X}$ generated by $\mathcal{S}$ (note that this reflects the *internal* behavior of $\mathcal{S}$). Then,

$$\limsup_{n\to\infty} \frac{\log(N'(n,\mathcal{S}))}{n} = \log \lambda_1(\boldsymbol{T}),$$

where $\boldsymbol{T}$ is the incidence matrix of $\mathcal{S}$.

Under a detectability condition of $\mathcal{S}$, the same result holds for behavioral entropy.

Definition 18 (Detectability): A transition system $\mathcal{S}$ is said to be l-detectable if there exists a finite $l \in \mathbb{N}$ such that, for each word $w \in \mathcal{B}^+(\mathcal{S})$, $|w| \geq l$, there exists a unique $x \in \mathcal{X}$ such that $w \in \mathcal{B}^+_x(\mathcal{S})$.

Theorem 8: Let $\mathcal{S}$ be an l-detectable finite-state system for some finite $l \in \mathbb{N}$, and let $\boldsymbol{T}$ be its incidence matrix. Then,

$$h(\mathcal{S}) = \log \lambda_1(\boldsymbol{T}). \tag{14}$$

Proof: Let $s := |\mathcal{Y}|$. Because of l-detectability, every $(n+l)$-long external behavior of $\mathcal{S}$ gives a unique n internal behavior, hence $N(n+l,\mathcal{S}) \geq N'(n,\mathcal{S})$. From every external behavior of length n, there can be at most s^l external behaviors of length $n+l$ (simply concatenate every possible word in $\mathcal{Y}^l$ to complete the length). Thus, $s^l N(n,\mathcal{S}) \geq N(n+l,\mathcal{S})$. Finally, since the output map H is single-valued, the number of external behaviors can never be bigger than the number of different internal behaviors: $N(n,\mathcal{S}) \leq N'(n,\mathcal{S})$. Combining these inequalities, the following holds for all $n > l$:

$$N(n,\mathcal{S}) \leq N'(n,\mathcal{S}) \leq s^l N(n,\mathcal{S}).$$

Now,

$$\begin{aligned}\limsup_{n\to\infty} \frac{\log(s^l N(n,\mathcal{S}))}{n} &= \limsup_{n\to\infty} \left(\frac{\log(s^l)}{n} + \frac{\log(N(n,\mathcal{S}))}{n}\right) \\ &= \limsup_{n\to\infty} \frac{\log(N(n,\mathcal{S}))}{n}.\end{aligned}$$

The sandwich rule and Theorem 7 conclude the proof. □

[9] In [25], the internal behavior from an initial state is called *itinerary*. The original theorem states that this quantity is also the topological entropy of the subshift $\mathcal{S}$, but here we only need the formula relating the limit to the spectral radius of $\boldsymbol{T}$.

Therefore, computing the behavioral entropy of a detectable finite transition system simply requires to compute the spectral radius of the associated graph. The following results help us apply Theorem 8 to the PETC traffic model.

Proposition 13: A nonblocking finite-state l-detectable autonomous transition system $\mathcal{S}$ has zero behavioral entropy if and only if all the SCCs of its associated graph are isolated nodes or simple cycles.

Proof: The spectrum of a digraph is the union of the spectra of its SCCs [33]. Because $\mathcal{S}$ is nonblocking, it must have at least one cycle. The adjacency matrix of an isolated node is $[\,0\,]$, thus, its spectrum is $\{0\}$. Furthermore, all vertices of a simple cycle have only one outgoing edge, hence the corresponding SCC has a constant outdegree of 1. From [33, Th. 2.1], the spectral radius of an SCC is 1 iff it has constant outdegree 1. Hence, the spectral radius of the whole graph is $\max(1,0) = 1$, whose log is 0. □

Remark 8: The l-complete PETC traffic model of Def. 13 is l-detectable because, by definition, each $k_1k_2\ldots k_l \in \mathcal{X}_l$ is the unique state that generates the finite behavior $hk_1, hk_2, \ldots hk_l$.

The following result establishes that the behavioral entropy of an l-complete abstraction bounds that of the concrete system. This implies that, if the abstraction is not behaviorally chaotic, the same holds for the concrete system.

Theorem 9: Consider the PETC system (1)–(3) ($\mathcal{T} = h\mathbb{N}$), its traffic model $\mathcal{S}$ from (11) and its l-complete traffic model (Def. 13) $\mathcal{S}_l$, with $l \in \mathbb{N}$. The following assertions are true:

i) $h(\mathcal{S}) \leq h(\mathcal{S}_l)$;

ii) If all SCCs of $\mathcal{S}_l$ are simple cycles, then $h(\mathcal{S}) = h(\mathcal{S}_l) = 0$, i.e., $\mathcal{S}$ is not chaotic.

Proof: Assertion (i): Proposition 10 gives that $\mathcal{S} \preceq \mathcal{S}_l$; then, from Theorem 5, $\mathcal{S} \preceq_{\mathcal{B}} \mathcal{S}_l$; finally, Proposition 12 concludes the proof.

Assertion (ii): $\mathcal{S}_l$ satisfies the premises of Proposition 13. Hence, $h(\mathcal{S}_l) = 0$. Using assertion (i) and the fact that $h(\mathcal{S}) \geq 0$, we conclude that $h(\mathcal{S}) = 0$. □

Revisiting Fig. 6, it is easy to see that $h(\mathcal{S}_1) = \log(2) = 1$ bit (base 2), while $h(\mathcal{S}_2) = 0$, which implies that the example of Fig. 4 is not chaotic.

E. Estimating and Computing Robust Metrics

Now we are equipped with the necessary tools to estimate robust limit metrics using an abstraction and determine when they are equal to the concrete system's or simply a lower bound. Based on the discussion in Section V-C, we define the following robust limit metric for the abstraction.

Definition 19 (Robust metric for $\mathcal{S}_l$): Consider system $\mathcal{S}$ from (11) and an l-complete model for it, $\mathcal{S}_l$ (Def. 13). Let $\tilde{\mathcal{B}}^\omega_{\text{au}}(\mathcal{S}_l)$ be the set of behaviors of $\mathcal{S}_l$ that are simple cycles in $\mathcal{S}_l$ and are absolutely unstable in $\mathcal{S}$. We define $\mathrm{Rob}V(\mathcal{S}_l)$ as $V(\mathcal{B}^\omega(\mathcal{S}_l) \setminus \tilde{\mathcal{B}}^\omega_{\text{au}}(\mathcal{S}_l))$.

Theorem 10: Consider system $\mathcal{S}$ from (11) and its l-complete model $\mathcal{S}_l$. Consider $V \in \{\mathrm{ILI}, \mathrm{ILA}\}$; then $\mathrm{Rob}V(\mathcal{S}_l) \leq \mathrm{Rob}V(\mathcal{S})$. Moreover, if all SCCs of $\mathcal{S}_l$ are simple cycles, and the minimizing cycle σ satisfies $\sigma^\omega \in \mathcal{B}^\omega(\mathcal{S})$, then $\mathrm{Rob}V(\mathcal{S}_l) = \mathrm{Rob}V(\mathcal{S})$.

Proof: Because all behaviors in $\tilde{\mathcal{B}}_{\text{au}}$ are absolutely unstable in $\mathcal{S}$, we have $\tilde{\mathcal{B}}^\omega_{\text{au}}(\mathcal{S}_l) \subseteq \mathcal{B}^\omega_{\text{au}}(\mathcal{S})$, and thus $\tilde{\mathcal{B}}^\omega_{\text{au}}(\mathcal{S}_l) \subseteq \mathcal{B}^\omega_{\text{u}}(\mathcal{S})$. From Proposition 10, $\mathcal{B}^\omega(\mathcal{S}_l) \supseteq \mathcal{B}^\omega(\mathcal{S})$; hence $\mathcal{B}^\omega(\mathcal{S}_l) \setminus \tilde{\mathcal{B}}^\omega_{\text{au}}(\mathcal{S}_l) \supseteq \mathcal{B}^\omega(\mathcal{S}) \setminus \mathcal{B}^\omega_{\text{u}}(\mathcal{S})$. Now, for any behavior set $\mathcal{B}$, $V(\mathcal{B}) = \inf\{f(y_i) \mid \{y_i\} \in \mathcal{B}\} = \inf\{F(\{y_i\}) \mid$

$\{y_i\} \in \mathcal{B}\}$, where $F(\{y_i\})$ is either $\liminf_{i\to\infty} y_i$ (ILI) or $\liminf_{n\to\infty} \frac{1}{n+1}\sum_{i=0}^{n} y_i$ (ILA). Hence, $\mathcal{B}_a \subseteq \mathcal{B}_b$ implies $V(\mathcal{B}_a) \geq V(\mathcal{B}_b)$, and the inequality $\mathrm{Rob}V(\mathcal{S}) \geq \mathrm{Rob}V(\mathcal{S}_l)$ follows.

For the equality: if $\mathcal{S}_l$ contains only simple cycles, then $\mathcal{S}$ is not behaviorally chaotic (Theorem 9), and thus $\mathcal{B}^\omega_{\mathrm{u}}(\mathcal{S}) = \mathcal{B}^\omega_{\mathrm{au}}(\mathcal{S})$ (all unstable cycles are absolutely unstable). Then, the minimizing cycle σ of $\mathcal{S}_l$ is by exclusion a stable cycle of $\mathcal{S}$. Since $\sigma^\omega \in \mathcal{B}^\omega(\mathcal{S}) \setminus \mathcal{B}^\omega_{\mathrm{u}}(\mathcal{S})$, we have that $\mathrm{Rob}V(\mathcal{S}_l) = F(\sigma^\omega) \geq \inf\{F(\{y_i\}) \mid \{y_i\} \in \mathcal{B}^\omega(\mathcal{S}) \setminus \mathcal{B}^\omega_{\mathrm{u}}(\mathcal{S})\} = \mathrm{Rob}V(\mathcal{S})$. Hence, $\mathrm{Rob}V(\mathcal{S}_l) = \mathrm{Rob}V(\mathcal{S})$. □

Revisiting Figs. 4 and 6 one last time, we have that $\mathrm{ILI}(\mathcal{S}) = \mathrm{ILA}(\mathcal{S}) = 1$, but using Theorem 10 on $\mathcal{S}_2$ we conclude that $\mathrm{Rob\,ILI}(\mathcal{S}) = \mathrm{Rob\,ILA}(\mathcal{S}) = 2$. Nevertheless, by Proposition 9, $\boldsymbol{M}(2)$ must be Schur, and hence a sampling period of $2\,h$ also stabilizes the system with the same traffic performance.

Remark 9: In the case of Rob ILI, if the invariant associated to the minimizing cycle σ can be verified to belong to a chaotic invariant set, under mild assumptions it holds that $\mathrm{Rob\,ILI}(\mathcal{S}_l) = \mathrm{Rob\,ILI}(\mathcal{S})$. To see this, first note that $\mathrm{Rob\,ILI} = \min(\sigma) =: y$; denoting by $\mathcal{X}_{\mathrm{c}}$ the chaotic invariant set, if $\mathcal{Q}_y \cap \mathcal{X}_{\mathrm{c}}$ has nonempty interior, by the Birkhoff Transitivity Theorem (see Def. 1) almost every solution starting in $\mathcal{X}_{\mathrm{c}}$ visits $\mathcal{Q}_y$ infinitely often.

Remark 10: In case a chaotic invariant set is ergodic, the infinimal limit average is the same almost everywhere (when restricted to the set), i.e., it is independent of the initial condition (as a consequence of Birkhoff Ergodic Theorem). As a matter of fact, almost everywhere means everywhere except the union of periodic orbits. Thus, $\mathrm{Rob\,ILA}(\mathcal{S}_l)$ can then be a conservative estimate. Nevertheless, the associated Rob ILA can be estimated through simulations. Ergodicity can be statistically tested using the approach of [34], where one tests whether the two initially different distributions on $\mathcal{X}$ converge to an equal one upon the repeated application of the map f by using a nonparametric hypothesis test such as the Kolmogorov–Smirnov test. Alternatively, the test can be performed on the distributions of outputs; because $\mathcal{Y}$ is discrete, one must use a hypothesis test suitable for discrete supports, such as the Cramér–von Mises (CvM) test [35]. For this approach to succeed, the initial distribution must contain only points that are in or lead to the chaotic invariant. The abstraction $\mathcal{S}_l$ can be used as an approximate selector of points on the chaotic invariant set, as its SCCs that are not simple cycles are related to overapproximations of potential chaotic invariants on the concrete system $\mathcal{S}$.

VI. Numerical Examples

We have implemented the methods to compute behavioral entropy and $\mathrm{Rob\,ILA}(\mathcal{S})$ using Theorem 10 in ETCetera [36], a Python toolbox to compute traffic abstractions of ETC systems.

Example 2: Consider system (1)–(3) with

$$\boldsymbol{A} = \begin{bmatrix} 0 & 1 \\ -2 & 3 \end{bmatrix}, \ \boldsymbol{B} = \begin{bmatrix} 0 \\ 1 \end{bmatrix},$$

$$c(s, \boldsymbol{x}, \hat{\boldsymbol{x}}) = |\boldsymbol{x} - \hat{\boldsymbol{x}}| > a|\boldsymbol{x}|, \qquad (9 \text{ revisited})$$

as in Example 1. Now we use PETC with $h = 0.05$ and check the following cases.

1) $\boldsymbol{K} = [0 \quad -5], a = 0.2$, as in Ex. 1 case 1.
2) $\boldsymbol{K} = [0 \quad -6], a = 0.2$.
3) $\boldsymbol{K} = [0 \quad -6], a = 0.32$, as in Ex. 1 case 2, and Fig. 3.

TABLE I
ILA Values for Example 2

Case	1	2	3
l (robust)	15 (15)	10 (10)	1 (10*)
ILA (RobILA)	0.137 (0.137)	0.1 (0.25)	0.1 (0.4)
CPU time (robust) [s]	50 (49)	23 (19)	0.81 (5655)

* Algorithm interrupted before finding a verified cycle.

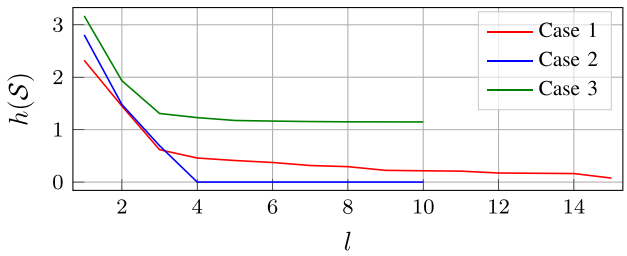

Fig. 7. Entropy $h(\mathcal{S}_l)$ as a function of l for Example 2.

Table I shows the values of ILA and RobILA for each case, as well as the l value at which the algorithms were terminated (or interrupted) and CPU times. Case 1 shows a periodic sequence σ^ω with $|\sigma| = 27$ that is stable and attains both the ILA and the RobILA, as well as $\mathrm{ILI} = \mathrm{Rob\,ILI} = 0.1$. In fact, case 1 exhibits only this cycle, and a bisimulation is found with $l = 27$. Case 2 is different in that an a.u. cycle is attained at $y = 0.1$, but a stable cycle has $y = 0.25$ (stationary). Upon inspection of $\mathcal{S}_l$, there is another stable cycle at $y = 0.3$. Unsurprisingly, we also obtain $\mathrm{ILI}(\mathcal{S}) = 0.1$ and $\mathrm{Rob\,ILI}(\mathcal{S}) = 0.25$, which happen at the same cycles. Finally, Case 3 is a chaotic example; the ILA is found at $y = \underline{\tau} = 0.1$ in the first iteration, but RobILA is never confirmed, although a lower bound of 0.4 is obtained, related to two unstable cycles, $(0.4)^\omega$ and $(0.35, 0.45)^\omega$. However, note the CPU time for obtaining the $\mathcal{S}_{10}$ abstraction of approximately 1.5 h (compare with the others of less than a minute): this is the effect of chaos on the refinements. As indicated by the entropy formula (12), the number of l-sized sequences grows exponentially with l. In fact, $\mathcal{S}_{10}$ has 9271 states, and an entropy of 1.14 bits. The SCC at which the two cycles belong has 7767 states, a strong indicative of a chaotic invariant set.

Fig. 7 shows the evolution of $h(\mathcal{S}_l)$ as a function of l for the three cases, where it is clear that the entropy seems to stabilize at a high value in Case 3, whereas it descends to zero in the other cases. Following Remark 10, two different initial distributions on states related to the large SCC of $\mathcal{S}_{10}$ where generated with 1000 points each, and after 9 iterations they converged to the same distribution (CvM test, $p = 0.998$), indicating that the chaotic invariant set is ergodic. The obtained ensemble average, which by Birkhoff Ergodic Theorem is equal to the limit average of any run starting in the invariant, is 0.417, slightly higher than the 0.4 using Theorem 10. Interestingly, 0.4 is a slightly higher limit average than what was obtained in the CETC implementation (Ex. 1 Case 3, and Remark 4), of 0.39; moreover, $\boldsymbol{M}(0.4)$ is not Schur, which highlights that the PETC has a larger average sampling period than any stabilizing periodic sampling. Finally, while $\mathrm{ILI}(\mathcal{S}) = \mathrm{ILA}(\mathcal{S}) = 0.1$ (at the same unstable cycle 0.1^ω) the best lower bound for RobILI is found to be 0.3,

which is witnessed by the unstable cycle $(0.3, 0.45, 0.4, 0.5)^\omega$. By inspection, the associated o-line belongs to the chaotic invariant, thus, by Remark 9 this is the correct value of Rob ILI$(\mathcal{S})$.

VII. Conclusion

ETC can exhibit very complex traffic patterns, and this seems to be more true the more "aggressive" the triggering mechanism w.r.t. sampling reduction. Simple traffic is observed on the opposite case. This is in line with the findings on [11] for $\mathbb{R}^2$, in which for small enough triggering parameters the states behave essentially like linear systems: two asymptotes, one stable and one unstable, or a spiral toward the origin when eigenvalues are complex conjugate. We have also seen an example of CETC whose robust ILA is higher than any stable periodic sampling strategy, whereas the same cannot happen with PETC under some generic assumptions. The first case is *a concrete example where ETC is more sampling-efficient than any periodic implementation.* At the same time, any practical implementation of it is effectively PETC, and as such any stable IST sequence it exhibits is stabilizing as a periodic sampling strategy; the only option for PETC to beat the most sampling-efficient periodic implementation involves chaotic or oscillatory traffic. This is not a problem per se: one could speculate that chaotic traffic could help in cyber-security aspects, but it can make scheduling multiple ETC loops in a network even more challenging.

A symbolic method for computing these robust limit metrics for PETC was presented in Section V. Despite its focus on linear systems, it applies to linearizable nonlinear systems if the controller renders the origin GES, as observed in [23]. Unfortunately, our method suffers from the curse of dimensionality, particularly when chaotic behaviors are present; future work includes using different abstractions that help pinpoint the existence of chaotic invariant sets. For the latter, an approach such as in [37] may be interesting, which can be seen in the framework of [1] as finding an abstraction that is *backwards* simulated by the concrete system.

While this work focuses on analysis, it is natural to ask how to use its results and methods for *synthesis* of efficient ETC systems. A straightforward way is to use it in a design-verify-adjust loop, but the insights of our results can be used more effectively. For example, one could design Tabuada's triggering parameter a, such that the conditions of Proposition 6 hold only for a sufficiently large IST. This topic is interesting for future work.

Admittedly, we have considered here the simple case of state-feedback without disturbances. It is known that output-feedback or external disturbances can severely alter the inter-sample behavior of the closed-loop system, potentially causing Zeno behavior [38], and practical modifications to the triggering condition are often necessary. It is an unclear whether adding these imperfections change our conclusions drastically, or if there are simple adjustments for these cases. Other important extensions involve considering time-regularized and dynamic triggering. The former seems easier, as it becomes essentially a combination of PETC (the state-space region triggering at the enforced minimal IST) and regular CETC; with this observation, most results of Section IV can be adapted. The latter can be more challenging, as the dynamics of the triggering parameter is often nonlinear. For perturbed systems, it is possible to extend the symbolic approach of this work by following the steps in [20]. Nevertheless, despite the simple case, we address here, we believe this work casts new light on the long-standing question of how relevant ETC is.

Appendix

A. Proof of Corollary 2

Proof: Assumption (i) combined with Theorem 2 implies that, if σ^ω is an output sequence of (7), then there exists a linear invariant $\mathcal{A}$ of $\boldsymbol{M}_\sigma$ s.t. $\mathcal{A} \subseteq \mathrm{cl}(\mathcal{Q}_\sigma)$. From (ii), any such $\mathcal{A}$ satisfies $\mathcal{A} \setminus \{\boldsymbol{0}\} \subseteq \mathcal{Q}_\sigma$, which by Theorem 2 implies σ^ω is an output sequence of (7). This establishes the equivalence.

To see that one such invariant $\mathcal{A}$ is either an o-line (1-dimensional) or an o-plane (2-dimensional), assume that it is higher dimensional. By assumption, $\boldsymbol{M}_\sigma$ is mixed, therefore, $\mathcal{A}$ is spanned by o-lines (associated with real eigenvalues) and o-planes (associated with complex conjugate pairs). Let $\boldsymbol{V} \in \mathbb{R}^{n_\mathrm{x} \times m}$ be a basis for $\mathcal{A}$ with $m > 2$, where the ith column of $\boldsymbol{V}$ is a real eigenvector of $\boldsymbol{M}_\sigma$ or, in case of a complex eigenvector pair $\boldsymbol{v}, \boldsymbol{v}^*$, the ith and $(i+1)$th columns are $\boldsymbol{v} + \boldsymbol{v}^*$ and $\mathrm{i}\boldsymbol{v} - \mathrm{i}\boldsymbol{v}^*$, respectively; these two columns form an invariant plane of $\boldsymbol{M}_\sigma$. In the former case, we have $\boldsymbol{V}\boldsymbol{E}_i = \boldsymbol{v}$, and in the latter, $\boldsymbol{V}\boldsymbol{E}_{i,i+1} = \begin{bmatrix} \boldsymbol{v} + \boldsymbol{v}^* & \mathrm{i}\boldsymbol{v} - \mathrm{i}\boldsymbol{v}^* \end{bmatrix}$, where $\boldsymbol{E}_i$ is a row matrix with the ith element being 1 and the rest zero, and $\boldsymbol{E}_{i,i+1} \in \mathbb{R}^{2\times m}$ has the entries $(1, i)$ and $(2, i+1)$ equal to 1, the rest being zero.

Since $\mathcal{Q}_\sigma$ is an intersection of sets of the form $\{\boldsymbol{x} \in \mathbb{R}^{n_\mathrm{x}} \mid \boldsymbol{x}^\mathsf{T}\boldsymbol{Q}_i\boldsymbol{x} \sim 0\}$, where $\sim \in \{=, \geq, >\}$, by Proposition 1, $\boldsymbol{V}^\mathsf{T}\boldsymbol{Q}_i\boldsymbol{V} \approx \boldsymbol{0}$ for every such $\boldsymbol{Q}_i$, where $\approx \in \{=, \succeq, \succ\}$, respectively. Since $\boldsymbol{A} \approx \boldsymbol{0} \Rightarrow \boldsymbol{B}^\mathsf{T}\boldsymbol{A}\boldsymbol{B} \approx \boldsymbol{0}$ for any non-singular $\boldsymbol{B}$, we can conclude that $\boldsymbol{V}^\mathsf{T}\boldsymbol{Q}_i\boldsymbol{V} \approx \boldsymbol{0}$ implies $(\boldsymbol{V}\boldsymbol{E}_i)^\mathsf{T}\boldsymbol{Q}_i(\boldsymbol{V}\boldsymbol{E}_i) \approx \boldsymbol{0}$ and $(\boldsymbol{V}\boldsymbol{E}_{i,i+1})^\mathsf{T}\boldsymbol{Q}_i(\boldsymbol{V}\boldsymbol{E}_{i,i+1}) \approx \boldsymbol{0}$, which imply that the corresponding o-line or o-plane is also a subset of $\mathcal{Q}_\sigma$. □

B. Proofs of Theorem 3 and Proposition 8

In these proofs, if f is not invertible in the pointwise sense, we treat its inverse in a set-based manner: $f^{-1} : \mathcal{Y} \rightrightarrows \mathcal{X}$, $f^{-1}(y) = \{x \in \mathcal{X} \mid f(x) = y\}$. In addition, here we work on the real projective space $\mathbb{P}^{n_\mathrm{x}-1}$, the space of all o-lines in $\mathbb{R}^{n_\mathrm{x}}$. The real projective space is the quotient of $\mathbb{R}^n \setminus \{\boldsymbol{0}\}$ by the relation $\boldsymbol{x} \sim \lambda\boldsymbol{x}, \lambda \in \mathbb{R} \setminus \{0\}$. Therefore, $\boldsymbol{x}$ and $\lambda\boldsymbol{x}$ are *the same point* $\boldsymbol{p} \in \mathbb{P}^{n_\mathrm{x}-1}$. We denote the natural projection of a point in $\mathbb{R}^{n_\mathrm{x}}$ onto $\mathbb{P}^{n_\mathrm{x}-1}$ by $h : \mathbb{R}^{n_\mathrm{x}} \setminus \{\boldsymbol{0}\} \to \mathbb{P}^{n_\mathrm{x}-1}$.

Lemma 2: Given f in (7), $g := h \circ f \circ h^{-1}$ is a well-defined function; moreover, if f is continuous, then g is continuous.

Proof: For any $\boldsymbol{p} \in \mathbb{P}^{n_\mathrm{x}-1}$, $h^{-1}(\boldsymbol{p})$ gives an o-line $\boldsymbol{l} \subset \mathbb{R}^{n_\mathrm{x}}$. From Proposition 2, it holds that $f(\boldsymbol{l}) = \boldsymbol{l}'$, where $\boldsymbol{l}'$ is also an o-line. Hence, $h(\boldsymbol{l}') = \boldsymbol{p}' \in \mathbb{P}^{n_\mathrm{x}-1}$, so g is well defined.

Continuity: f is also continuous for o-lines, i.e., if $\boldsymbol{l}$ is an o-line, $\lim_{\boldsymbol{l}' \to \boldsymbol{l}} f(\boldsymbol{l}') = \boldsymbol{l}$; hence, $\lim_{\boldsymbol{p}' \to \boldsymbol{p}} g(\boldsymbol{p}') = \boldsymbol{p}$. □

Proof of Theorem 3: Every continuous map from the real projective space to itself has a fixed point if its dimension is even [38, p. 109]. From Lemma 2, $g : \mathbb{P}^{n_\mathrm{x}-1} \to \mathbb{P}^{n_\mathrm{x}-1}$ is a continuous function; thus, g has a fixed point if n_x is *odd*.

Now we need to show that, if g has a fixed point, then f has a fixed o-line. If $\boldsymbol{p}$ is a fixed point of g, then take a point $\boldsymbol{x} \in h^{-1}(\boldsymbol{p})$. Then, $h(f(\boldsymbol{x})) = g(h(\boldsymbol{x})) = \boldsymbol{p} \therefore f(\boldsymbol{x}) \in h^{-1}(\boldsymbol{p})$ Hence, there exists $\boldsymbol{x}' \in h^{-1}(\boldsymbol{p})$ satisfying $\boldsymbol{x}' = f(\boldsymbol{x})$, where $\boldsymbol{x}' = \lambda \boldsymbol{x}$, for some λ. Since f is homogeneous as per Proposition 2, $\boldsymbol{x}' = f(\boldsymbol{x})$ is true for any $\boldsymbol{x}$ in the o-line containing it. Hence, this line is fixed by f, and the proof is complete. □

Proof of Proposition 8: From Lemma 2, $g : \mathbb{P}^{n_x-1} \to \mathbb{P}^{n_x-1}$ is well defined. Fix $\boldsymbol{x} \in \boldsymbol{l}$ and let $\boldsymbol{p} := h(\boldsymbol{x})$. We want to show that there is a coordinate system for the tangent space of g at $\boldsymbol{p}$ such that the Jacobian of g at $\boldsymbol{p}$ is equal to $\frac{1}{\lambda}\boldsymbol{O}_{\boldsymbol{x}}{}^{\mathsf{T}} J_f(\boldsymbol{x}) \boldsymbol{O}_{\boldsymbol{x}}$.

First, note that the real projective space is locally equal to the unit sphere, hence, we can use the orthogonal subspace to a unitary $\boldsymbol{x}$ within $\boldsymbol{l}$ as the tangent subspace of $\boldsymbol{p}$ embedded in $\mathbb{R}^{n_x}$. Denote it as $\mathcal{T}(\boldsymbol{x})$. Let $\boldsymbol{d}$ be a unitary vector orthogonal to $\boldsymbol{x}$. Any point in $\mathcal{T}(\boldsymbol{x})$ can be described as $\boldsymbol{x} + a\boldsymbol{d}$. To get the Jacobian of g, we apply f to $\boldsymbol{x} + h\boldsymbol{d}$ and project the result back to $\mathcal{T}(\boldsymbol{x})$.

$$\begin{aligned} f(\boldsymbol{x} + h\boldsymbol{d}) &= f(\boldsymbol{x}) + hJ_f(\boldsymbol{x})\boldsymbol{d} + \mathcal{O}(h^2) \\ &= \lambda \boldsymbol{x} + hJ_f(\boldsymbol{x})\boldsymbol{d} + \mathcal{O}(h^2), \end{aligned}$$

whose projection back to $\mathcal{T}(\boldsymbol{x})$ is simply $\boldsymbol{x} + h/\lambda \cdot J_f(\boldsymbol{x})\boldsymbol{d} + \mathcal{O}(h^2)$. Thus, the vector of variation of g w.r.t. $\boldsymbol{d}$ embedded in $\mathbb{R}^{n_x}$ is

$$\lim_{h\to 0} \frac{\boldsymbol{x} + h/\lambda \cdot J_f(\boldsymbol{x})\boldsymbol{d} + \mathcal{O}(h^2) - \boldsymbol{x}}{h} = \frac{1}{\lambda} J_f(\boldsymbol{x})\boldsymbol{d}.$$

Now let $\boldsymbol{d}_i$ be the ith column of $\boldsymbol{O}_{\boldsymbol{x}}$. Every $\boldsymbol{d}_i$ is unitary and orthogonal to $\boldsymbol{x}$. Setting $\boldsymbol{d}_1, \boldsymbol{d}_2, \ldots \boldsymbol{d}_{n_x-1}$ as a coordinate system for the tangent space of g at $\boldsymbol{p}$, the component of the derivative of g on $\boldsymbol{d}_j$ from a variation in $\boldsymbol{d}_i$ is $\boldsymbol{d}_j^{\mathsf{T}} \frac{1}{\lambda} J_f(\boldsymbol{x})\boldsymbol{d}_i$; putting in matrix form, we arrive at $J_g(\boldsymbol{p}) = \frac{1}{\lambda}\boldsymbol{O}_{\boldsymbol{x}}{}^{\mathsf{T}} J_f(\boldsymbol{x})\boldsymbol{O}_{\boldsymbol{x}}$, which implies local attractivity if Schur. □

C. Proof of Theorem 4

We start by introducing the following lemma.

Lemma 3: Let $\boldsymbol{N} \in \mathbb{S}^n$ be a symmetric matrix, and let (P, N, Z) be its signature, i.e., the number of its positive, negative, and zero eigenvalues, respectively. Let m be a positive integer s.t. $m \leq n$. The following holds.

i) There is an m-dimensional linear space $\mathcal{A}$ such that $\boldsymbol{x} \in \mathcal{A} \setminus \{0\} \Rightarrow \boldsymbol{x}^{\mathsf{T}}\boldsymbol{N}\boldsymbol{x} > 0$ if and only if $\boldsymbol{N}$ has at least m positive eigenvalues.

ii) There is an m-dimensional linear space $\mathcal{A}$ such that $\boldsymbol{x} \in \mathcal{A} \Rightarrow \boldsymbol{x}^{\mathsf{T}}\boldsymbol{N}\boldsymbol{x} = 0$ if and only if $\min(P + Z, N + Z) \geq m$. As a consequence $n \geq 2m - Z$.

Proof: (i) This is a trivial consequence of Sylvester's law of inertia (see [40, Ch. XV.4]).

(ii) Based on Proposition 1, this is equivalent to $\boldsymbol{V}^{\mathsf{T}}\boldsymbol{N}\boldsymbol{V} = \boldsymbol{0}$, for some $\boldsymbol{V} \in \mathbb{R}^{n\times m}$.

Proof of necessity: We assume that some full-rank $\boldsymbol{V} \in \mathbb{R}^{n\times m}$ satisfies $\boldsymbol{V}^{\mathsf{T}}\boldsymbol{N}\boldsymbol{V} = \boldsymbol{0}$ and prove that $\min(P + Z, N + Z) \geq m$. Using Sylvester's law of inertia, we can write $\boldsymbol{N} = \boldsymbol{T}^{\mathsf{T}}\boldsymbol{S}\boldsymbol{T}$, where $\boldsymbol{S}$ is diagonal containing only 1, 0 and -1 entries in the diagonal, with counts P, Z, and N, respectively, and $\boldsymbol{T}$ is invertible. If $Z \geq m$, $\min(P + Z, N + Z) \geq m$ is trivially satisfied. Let us now assume that $Z < m$. Then, $\boldsymbol{V}^{\mathsf{T}}\boldsymbol{N}\boldsymbol{V} = \begin{bmatrix}\boldsymbol{W}_0 \\ \boldsymbol{W}_1\end{bmatrix}^{\mathsf{T}} \begin{bmatrix}\boldsymbol{0} & \boldsymbol{0} \\ \boldsymbol{0} & \bar{\boldsymbol{S}}\end{bmatrix} \begin{bmatrix}\boldsymbol{W}_0 \\ \boldsymbol{W}_1\end{bmatrix}$, where $\begin{bmatrix}\boldsymbol{W}_0 \\ \boldsymbol{W}_1\end{bmatrix} := \boldsymbol{T}\boldsymbol{V}$ is partitioned according to the zero and the nonzero ($\bar{\boldsymbol{S}}$) parts of $\boldsymbol{S}$, and it also has rank m. Thus, $\boldsymbol{W}_0$ has rank Z and $\boldsymbol{W}_1$ has rank $m - Z$. Let $\boldsymbol{W}_2 := \bar{\boldsymbol{S}}\boldsymbol{W}_1$. Pre-multiplying $\boldsymbol{W}_2$ by $\bar{\boldsymbol{S}}$, we get $\bar{\boldsymbol{S}}\boldsymbol{W}_2 = \bar{\boldsymbol{S}}^2\boldsymbol{W}_1 = \boldsymbol{W}_1$ (note that $\bar{\boldsymbol{S}}^2 = \mathbf{I}$). Thus, we can write

$$\bar{\boldsymbol{S}}\begin{bmatrix}\boldsymbol{W}_1 & \boldsymbol{W}_2\end{bmatrix} = \bar{\boldsymbol{S}}\boldsymbol{W} = \begin{bmatrix}\boldsymbol{W}_2 & \boldsymbol{W}_1\end{bmatrix} = \boldsymbol{W}\boldsymbol{P}$$

where $\boldsymbol{P} := \begin{bmatrix}\boldsymbol{0} & \mathbf{I} \\ \mathbf{I} & \boldsymbol{0}\end{bmatrix}$ is a permutation matrix of dimension $2(m - Z)$. This matrix has $m - Z$ eigenvalues in 1 and $m - Z$ eigenvalues in -1. Now, take one pair $(\lambda, \boldsymbol{x})$ such that $\boldsymbol{P}\boldsymbol{x} = \lambda\boldsymbol{x}$. Then, $\bar{\boldsymbol{S}}\boldsymbol{W}\boldsymbol{x} = \boldsymbol{W}\boldsymbol{P}\boldsymbol{x} = \lambda\boldsymbol{W}\boldsymbol{x}$, so λ is also an eigenvalue of $\bar{\boldsymbol{S}}$. Thus, $\boldsymbol{S}$ has at least $m - Z$ eigenvalues equal to 1 and $m - Z$ equal to -1. Therefore, $\min(P + Z, N + Z) \geq m$.

Proof of sufficiency: Now we start with a symmetric $\boldsymbol{N}$ satisfying $\min(P + Z, N + Z) \geq m$, and then construct $\boldsymbol{V} \in \mathbb{R}^{n\times m}$ such that $\boldsymbol{V}^{\mathsf{T}}\boldsymbol{N}\boldsymbol{V} = \boldsymbol{0}$. Take the Sylvester matrix $\boldsymbol{S}$ of $\boldsymbol{N}$ and select its rows and columns such that the obtained submatrix has $\bar{Z} := \min(Z, m)$ zero entries, $\max(m - Z, 0)$ entries equal to 1 and $\max(m - Z, 0)$ entries equal to -1. Denote this submatrix by $\bar{\boldsymbol{S}}$. We have that that there exists $\bar{\boldsymbol{W}} \in \mathbb{R}^{(2m-\bar{Z})\times(2m-\bar{Z})}$ such that $\bar{\boldsymbol{W}}^{-1}\bar{\boldsymbol{S}}\bar{\boldsymbol{W}} = \begin{bmatrix}\boldsymbol{0} & \boldsymbol{0} \\ \boldsymbol{0} & \boldsymbol{P}\end{bmatrix}$, where $\boldsymbol{P}$ is the same permutation matrix as in the proof of necessity ($\bar{\boldsymbol{W}}$ comes from the eigendecomposition of $\begin{bmatrix}\boldsymbol{0} & \boldsymbol{0} \\ \boldsymbol{0} & \boldsymbol{P}\end{bmatrix}$). Build $\boldsymbol{W} := \begin{bmatrix}\bar{\boldsymbol{W}} \\ \boldsymbol{0}\end{bmatrix}$ s.t. $\boldsymbol{W} \in \mathbb{R}^{n\times(2m-\bar{Z})}$, and denote its first m columns of $\bar{\boldsymbol{W}}$ by $\boldsymbol{W}_1$. Using the same arguments as in the proof of necessity, the matrix $\boldsymbol{V} = \boldsymbol{T}^{-1}\boldsymbol{W}_1$ satisfies $\boldsymbol{V}^{\mathsf{T}}\boldsymbol{N}\boldsymbol{V} = \boldsymbol{0}$.

Finally, $P + Z \geq m$ and $N + Z \geq m$ imply (by addition) $P + N + 2Z = n + Z \geq 2\,m$. Hence, $n \geq 2m - Z$. □

Proof of Theorem 4: Case (i) is trivial, because the only o-plane is the whole $\mathbb{R}^2$, which being isochronous implies periodic sampling. Conversely, it is necessary that $n_x \geq 3$ if we are interested in nontrivial cases. What remains to be shown is that $n_x = 3$ in CETC implies that $N(\tau)$ is singular if an o-plane is isochronous with IST τ.

For CETC, the isochronous set $\mathcal{Q}_\tau$ contains a set of the form $\{\boldsymbol{x} \in \mathbb{R}^{n_x} \mid \boldsymbol{x}^{\mathsf{T}}\boldsymbol{N}(\tau)\boldsymbol{x} = 0\}$. As we are looking for o-planes, we apply Lemma 3 (ii) with $m = 2$. Suppose that $n_x = 3$ and $\boldsymbol{N}(\tau)$ is not singular, i.e., $Z = 0$; then, by Lemma 3 (ii), $\boldsymbol{N}(\tau)$ must have at least two positive and two negative eigenvalues, implying that $n_x \geq 4$. This is a contradiction; therefore, either $\boldsymbol{N}(\tau)$ is singular, proving case (ii), or $n_x \geq 4$, proving case (iii). □

D. Proof of Proposition 11

First we introduce the following Lemma.

Lemma 4: Let $\boldsymbol{\xi}(k + 1) = \boldsymbol{M}\boldsymbol{\xi}(k)$ be a linear autonomous system, $\boldsymbol{M}$ mixed, and let $\boldsymbol{v}_1, \boldsymbol{v}_2, \ldots, \boldsymbol{v}_n$ be the unitary eigen-

vectors of $\boldsymbol{M}$ ordered from largest-in-magnitude corresponding eigenvalue to smallest. Denote by $\mathcal{A}$ any linear invariant of $\boldsymbol{M}$ containing $\boldsymbol{v}_1$. Then, for every initial state $\boldsymbol{\xi}(0) = a_1\boldsymbol{v}_1 + \cdots = a_n\boldsymbol{v}_n$ where $a_1 \neq 0$, it holds that $\lim_{k\to\infty} \frac{\boldsymbol{\xi}(k)}{|\boldsymbol{\xi}(k)|} \in \mathcal{A}$.

Proof: This is trivial consequence of the proof of [22, Lemma 3] when $a_1 \neq 0$. □

Lemma 4 paraphrases the known fact that almost every trajectory of a linear system converges to its dominant mode.

Proof of Proposition 11. Item (I): For contradiction, assume that σ^ω is stable, and let $m := |\sigma|$. First, we check $\boldsymbol{x}_0 \in \mathcal{Q}_\sigma$. In this case, the samples $\{\boldsymbol{x}_i\}$ evolve according to $\boldsymbol{x}_{i+m} = \boldsymbol{M}_\sigma \boldsymbol{x}_i$. Let $\boldsymbol{x}_0 = a_1\boldsymbol{v}_1 + \cdots = a_n\boldsymbol{v}_n$ where $\boldsymbol{v}_j$ are the eigenvectors of $\boldsymbol{M}_\sigma$ ordered as in Lemma 4. For any $\boldsymbol{x}_0 \in \mathbb{R}^n$ almost all points in its neighborhood satisfy $a_1 \neq 0$. Hence, by Lemma 4, $\lim_{i\to\infty} \frac{\boldsymbol{x}_{mi}}{|\boldsymbol{x}_{mi}|} \in \mathcal{A}$, but $\mathcal{A} \nsubseteq \mathrm{cl}(\mathcal{Q}_\sigma)$. Thus, $\{\boldsymbol{x}_{mi}\}$ escapes $\mathcal{Q}_\sigma$ at a some finite i, hence, $\{y(\boldsymbol{x}_{mi})\} \neq \sigma^\omega$. This contradicts the assumption that σ^ω is stable.

We now see that the set of states $\boldsymbol{x}$ such that $\mathcal{B}^\omega_{\boldsymbol{x}}(\mathcal{S}) = \alpha\sigma^\omega$, $|\alpha| < \infty$ has measure zero. This is done by induction on the length of α. Let $\mathcal{X}_m$ be the set of states whose behavior is if $\alpha\sigma^\omega$ with $|\alpha| = m$. If $m = 0$, we have already seen that $\mathcal{X}_0$ is a linear invariant of $\boldsymbol{M}_\sigma$; because this linear subspace does not contain $\boldsymbol{v}_1$, it has zero measure. Now assume $\mathcal{X}_m$ has zero measure. The set $\mathcal{X}_{m+1}$ is the pre-image of $\mathcal{X}_m$, hence, $\mathcal{X}_{m+1} \subseteq \cup_{k=1}^{\bar{k}} \boldsymbol{M}_k^{-1}\mathcal{X}_m$. Because $\boldsymbol{M}_k$ is nonsingular and the union is finite, $\mathcal{X}_{m+1}$ is also measure zero. This concludes the proof that σ^ω is unstable.

Item (II): First, note that c must be a multiple of $|\sigma|$. Let α be any l-long subsequence of σ^ω. We have already seen that for almost every $\boldsymbol{x} \in \mathcal{Q}_\alpha$ there exists a finite k such that the solution to (7) $\boldsymbol{\xi}_{\boldsymbol{x}}(ck-1) \notin \mathcal{Q}_\alpha$. To prove absolutely instability, it suffices to check the behavior from any such $\boldsymbol{\xi}_{\boldsymbol{x}}(ck-1)$ does not contain σ^L for some L large enough. We show that it is true with $L = c/|\sigma|$.

Let $\mathcal{C}$ be the simple-cycle SCC formed by $\{x_1, x_2, \ldots, x_c\}$. Since $\alpha \in \mathcal{C}$, w.l.o.g., let $x_1 = \alpha$, which is related to $\boldsymbol{x}$. Let $\boldsymbol{x}' := \boldsymbol{\xi}_{\boldsymbol{x}}(ck)$ and take x' as the unique state in $\mathcal{S}_l$ related to $\boldsymbol{x}'$, respectively. We first show that $x' \notin \mathcal{C}$: since there is a run from $\boldsymbol{x}$ to $\boldsymbol{x}'$ with length ck, there must be a run segment of length ck from x_1 to x'. Because $\mathcal{C}$ is strongly connected, if $x' \in \mathcal{C}$, the only path would be $(x_1 \ldots x_c)^k x_1$, hence, $x' = x_1$. But this is a contradiction because $x' \neq \alpha$ since $\boldsymbol{\xi}_{\boldsymbol{x}}(ck-1) \notin \mathcal{Q}_\alpha$. Thus, $x' \notin \mathcal{C}$.

Now, there is no path in the abstraction connecting x' to $\mathcal{C}$ (otherwise $\mathcal{C}$ would not be a simple cycle). Therefore, because $\mathcal{S}_l \succeq \mathcal{S}$, it is trivial to see that there is also no path from $\boldsymbol{x}'$ back to $\mathcal{Q}_\alpha$, i.e., $\boldsymbol{\xi}_{\boldsymbol{x}'}(k) \notin \mathcal{Q}_\alpha, \forall k \in \mathbb{N}$. Thus, $\mathcal{B}^\omega_{\boldsymbol{x}'}(\mathcal{S})$ does not contain σ^L as a subsequence, concluding the proof. □

ACKNOWLEDGMENT

The authors would like to thank Dr. Giannis Delimpaltadakis for his fundamental comments in the first version, and the anonymous reviewers for the excellent feedback provided.

REFERENCES

[1] P. Tabuada, "Event-triggered real-time scheduling of stabilizing control tasks," *IEEE Trans. Autom. Control*, vol. 52, no. 9, pp. 1680–1685, Sep. 2007.
[2] R. E. Hufnagel, "Analysis of cyclic-rate sampled-data feedback-control systems," *Trans. Amer. Inst. Elect. Engineers, Part II: Appl. Ind.*, vol. 77, no. 5, pp. 421–425, Nov. 1958.
[3] K. J. Åström and B. Bernhardsson, "Comparison of Riemann and Lebesgue sampling for first order stochastic systems," in *Proc. IEEE 41st Conf. Decis. Control*, 2002, vol. 2, pp. 2011–2016.
[4] X. Wang and M. D. Lemmon, "Event design in event-triggered feedback control systems," in *Proc. IEEE 47th Conf. Decis. Control*, 2008, pp. 2105–2110.
[5] A. Girard, "Dynamic triggering mechanisms for event-triggered control," *IEEE Trans. Autom. Control*, vol. 60, no. 7, pp. 1992–1997, Jul. 2015.
[6] W. P. M. H. Heemels, K. H. Johansson, and P. Tabuada, "An introduction to event-triggered and self-triggered control," in *Proc. IEEE 51st Conf. Decis. Control*, 2012, pp. 3270–3285.
[7] W. P. M. H. Heemels, M. C. F. Donkers, and A. R. Teel, "Periodic event-triggered control for linear systems," *IEEE Trans. Autom. Control*, vol. 58, no. 4, pp. 847–861, Apr. 2013.
[8] R. Goebel, R. G. Sanfelice, and A. R. Teel, *Hybrid Dynamical Systems: Modeling, Stability, and Robustness*. Princeton, NJ, USA: Princeton Univ. Press, 2012.
[9] S. Linsenmayer and F. Allgöwer, "Performance oriented triggering mechanisms with guaranteed traffic characterization for linear discrete-time systems," in *Proc. Eur. Control Conf.*, 2018, pp. 1474–1479.
[10] M. Velasco, P. Martí, and E. Bini, "Equilibrium sampling interval sequences for event-driven controllers," in *Proc. Eur. Control Conf.*, 2009, pp. 3773–3778.
[11] R. Postoyan, R. G. Sanfelice, and W. P. M. H. Heemels, "Inter-event times analysis for planar linear event-triggered controlled systems," in *Proc. IEEE 58th Conf. Decis. Control*, 2019, pp. 3601–3606.
[12] A. Rajan and P. Tallapragada, "Analysis of inter-event times for planar linear systems under a general class of event triggering rules," in *Proc. IEEE 59th Conf. Decis. Control*, 2020, pp. 5206–5211.
[13] R. Postoyan, R. G. Sanfelice, and W. Heemels, "Explaining the 'mystery' of periodicity in inter-transmission times in two-dimensional event-triggered controlled system," *IEEE Trans. Autom. Control*, vol. 68, no. 2, pp. 912–927, Feb. 2023.
[14] P. Tabuada, *Verification and Control of Hybrid Systems: A Symbolic Approach*. Berlin, Germany: Springer, 2009.
[15] A. S. Kolarijani and M. Mazo Jr, "A formal traffic characterization of LTI event-triggered control systems," *IEEE Trans. Control Netw. Syst.*, vol. 5, no. 1, pp. 274–283, Mar. 2018.
[16] M. Mazo Jr, A. S. Kolarijani, D. Adzkiya, and C. Hop, "Abstracted models for scheduling of event-triggered control data traffic," in *Proc. Control Subject Comput. Commun. Constraints*, 2018, pp. 197–217.
[17] A. Fu and M. Mazo Jr, "Traffic models of periodic event-triggered control systems," *IEEE Trans. Autom. Control*, vol. 64, no. 8, pp. 3453–3460, Aug. 2019.
[18] G. A. Gleizer and M. MazoJr., "Scalable traffic models for scheduling of linear periodic event-triggered controllers," *IFAC-PapersOnLine*, vol. 53, no. 2, pp. 2726–2732, 2020.
[19] G. Delimpaltadakis and M. Mazo Jr, "Traffic abstractions of nonlinear homogeneous event-triggered control systems," in *Proc. IEEE 59th Conf. Decis. Control*, 2020, pp. 4991–4998.
[20] G. Delimpaltadakis and M. Mazo Jr, "Abstracting the traffic of nonlinear event-triggered control systems," *IEEE Trans. Autom. Control*, to be published, doi: 10.1109/TAC.2022.3195128.
[21] G. A. Gleizer and M. Mazo Jr, "Towards traffic bisimulation of linear periodic event-triggered controllers," *IEEE Control Syst. Lett.*, vol. 5, no. 1, pp. 25–30, Jan. 2021.
[22] G. A. Gleizer and M. Mazo Jr, "Computing the sampling performance of event-triggered control," in *Proc. 24th Int. Conf. Hybrid Syst., Comput. Control*, 2021, pp. 1–7.
[23] G. A. Gleizer and M. Mazo Jr, "Computing the average inter-sample time of event-triggered control using quantitative automata," *Nonlinear Anal.: Hybrid Syst.*, vol. 47, 2023, Art. no. 101290.
[24] K. Chatterjee, L. Doyen, and T. A. Henzinger, "Quantitative languages," *ACM Trans. Comput. Log.*, vol. 11, no. 4, pp. 1–38, 2010.

[25] C. Robinson, *Dynamical Systems: Stability, Symbolic Dynamics, and Chaos. Studies in Advanced Mathematics*. Boca Raton, FL, USA: CRC-Press, 1999.
[26] G. A. Gleizer and M. Mazo Jr, "Self-triggered output feedback control for perturbed linear systems," *IFAC-PapersOnLine*, vol. 51, no. 23, pp. 248–253, 2018.
[27] M. Mazo Jr, A. Anta, and P. Tabuada, "An ISS self-triggered implementation of linear controllers," *Automatica*, vol. 46, no. 8, pp. 1310–1314, 2010.
[28] W. de Melo and S. van Strien, *One-Dimensional Dynamics*. Berlin, Germany: Springer, 2012.
[29] R. M. Karp, "A characterization of the minimum cycle mean in a digraph," *Discr. Math.*, vol. 23, no. 3, pp. 309–311, 1978.
[30] M. Chaturvedi and R. M. McConnell, "A note on finding minimum mean cycle," *Inf. Process. Lett.*, vol. 127, pp. 21–22, 2017.
[31] A.-K. Schmuck, P. Tabuada, and J. Raisch, "Comparing asynchronous l-complete approximations and quotient based abstractions," in *Proc. IEEE 54th Conf. Decis. Control*, 2015, pp. 6823–6829.
[32] J. C. Willems, "Paradigms and puzzles in the theory of dynamical systems," *IEEE Trans. Autom. Control*, vol. 36, no. 3, pp. 259–294, Mar. 1991.
[33] R. A. Brualdi, "Spectra of digraphs," *Linear Algebra Appl.*, vol. 432, no. 9, pp. 2181–2213, 2010.
[34] I. Domowitz and M. A. El-Gamal, "A consistent test of stationary-ergodicity," *Econometric Theory*, vol. 9, no. 4, pp. 589–601, 1993.
[35] T. B. Arnold and J. W. Emerson, "Nonparametric goodness-of-fit tests for discrete null distributions," *R. J.*, vol. 3, no. 2, pp. 34–39, 2011.
[36] G. Delimpaltadakis, G. A. Gleizer, I. van Straalen, and M. Mazo Jr., "ETCetera: Beyond event-triggered control," in *Proc. 25th ACM Int. Conf. Hybrid Syst.: Comput. Control*, 2022, pp. 1–11.
[37] S. Day, R. Frongillo, and R. Trevino, "Algorithms for rigorous entropy bounds and symbolic dynamics," *SIAM J. Appl. Dynamical Syst.*, vol. 7, no. 4, pp. 1477–1506, 2008.
[38] D. Borgers and W. Heemels, "Event-separation properties of event-triggered control systems," *IEEE Trans. Autom. Control*, vol. 59, no. 10, pp. 2644–2656, Oct. 2014.
[39] A. Granas and J. Dugundji, *Fixed Point Theory*. Berlin, Germany: Springer, 2003.
[40] S. Lang, *Algebra*. New York, NY, USA: Springer, 2005.

Gabriel de Albuquerque Gleizer (Member, IEEE) received the control and automation engineering degree in 2010 and the M.Sc. degree in electrical engineering in 2013 from the Federal University of Rio de Janeiro, Rio de Janeiro, Brazil, and the Ph.D. (*cum laude*) degree in systems and control from the Delft Center for Systems and Control (DCSC), Delft University of Technology (TU Delft), Delft, The Netherlands, in 2022.

He is currently a Postdoctoral Researcher with DCSC, TU Delft. Before his Ph.D. degree, he was a Research Engineer with GE Global Research with Rio de Janeiro, Brazil, from 2012 to 2017. His main research interests are hybrid systems, fault diagnosis, networked control systems, and formal methods for (quantitative) analysis and control.

Manuel Mazo Jr. (Senior Member, IEEE) received the telecommunications engineering "Ingeniero" degree from the Polytechnic University of Madrid, Madrid, Spain, in 2003, the "Civilingenjör" degree in electrical engineering from the Royal Institute of Technology, Stockholm, Sweden, in 2003, and the M.Sc. and Ph.D. degrees in electrical engineering from the University of California, Los Angeles, CA, USA, in 2007 and 2010, respectively.

He is currently an Associate Professor with the Delft Center for Systems and Control, Delft University of Technology, Delft, The Netherlands. Between 2010 and 2012, he held a joint Postdoctoral Position with the University of Groningen, Groningen, The Netherlands, and the innovation centre INCAS3, The Netherlands. His main research interests include the formal study of problems emerging in modern control system implementations and, in particular, the study of networked control systems and the application of formal verification and synthesis techniques to control.

Dr. Mazo was the recipient of a University of Newcastle Research Fellowship (2005), the Spanish Ministry of Education/UCLA Fellowship (2005–2009), the Henry Samueli Scholarship from the UCLA School of Engineering and Applied Sciences (2007/2008), and an ERC Starting Grant (2017).